UC Riverside

UCR Honors Capstones 2025-2026

Title

ROLE OF ECDYSIS TRIGGERING HORMONE IN DROSOPHILA COURTSHIP SUCCESS

Permalink

https://escholarship.org/uc/item/7p48d8bm

Author

Vijaya Kumar, Likhith

Publication Date

2026-06-15

eScholarship.org Powered by the California Digital Library
University of California

ROLE OF ECDYSIS TRIGGERING HORMONE IN *DROSOPHILA* COURTSHIP SUCCESS

By

Likhith Vijaya Kumar

A capstone project submitted for Graduation with University Honors

May 7, 2026

University Honors

University of California, Riverside

APPROVED

Dr. Michael E. Adams

Department of Entomology and Molecular, Cell, and Systems Biology

Dr. Begoña Echeverria, Howard H. Hays, Jr. Chair

University Honors

ABSTRACT

Ecdysis, the intricate process by which insects shed their exoskeleton, is initiated by ecdysis-triggering hormone (ETH) secreted from endocrine Inka cells. While ETH is essential for the successful developmental sequence leading to adulthood, recent evidence indicates that this hormone is re-purposed for adult functions, including reproductive physiology and behavior. Prior work has revealed that adult ETH signaling plays a major role in modulating post-copulation courtship inhibition (PCCI). I have found that heat stress appears to create ETH deficiency and reduced courtship success. Furthermore, promotion of Inka cell secretory activity rescues behavior. Using the GAL4/UAS system, I express either CsChrimson or dTRPA1 in Inka cells to evoke ETH release with light or temperature, respectively, following heat-stress exposure. Courtship is quantified with a standard courtship index and ethogram-based scoring of sequential behaviors, complemented by automated tracking to extract velocity and locomotor trajectory measurements. Our findings support the hypothesis that stress reduces successful copulation and that conditional ETH release rescues this phenotype. These studies further define the essential role of ETH for adult reproductive success, in particulalar male *Drosophila melanogaster* courtship behavior. Our findings also motivate future studies involving interconnected hormones such as Juvenile Hormone and Ecdysone.

ACKNOWLEDGEMENTS

I thank Dr. Michael E. Adams for his mentorship, guidance, and the opportunity to work on this project. I thank Cameron Zappetta for his support in answering questions and explaining key concepts throughout the project. I thank Aiden Bryan, Arghavan Maleki, Amy Quach, and Dylan Pak for their help with experimental preparation and fly maintenance. I also thank the University Honors Program staff and faculty for their support during this project.

TABLE OF CONTENTS

Background……..5

Significance……..7

Methods……..10

Results……15

Discussion……..20

Current Work and Future Directions……..23

Conclusions……25

References……..26

Figures……29

BACKGROUND

Ecdysis Triggering Hormone (ETH) is a peptide released from epitracheal Inka cells in all insect species examined thus far. It was first identified as an essential driver of ecdysis, the process by which insects shed their exoskeleton at the end of each developmental stage (Park et al., 2002). Inka cells are specialized endocrine cells positioned alongside the tracheal system, where they release ETH directly into the circulating hemolymph for systemic distribution to target tissues throughout the body. In *Drosophila melanogaster*, the ETH gene encodes a single prepro-ETH precursor that is enzymatically cleaved into three distinct products (Figure 1)(Park et al., 1999). The first product, ETH-1, serves as the primary regulator of ecdysis behavior. The second product, ETH-2, plays a secondary role in ecdysis control and exhibits variable potency depending on the target tissue. The third product, ETH-AP, is generated as a side product of precursor processing and has no clearly established function. Once released into circulation, ETH-1 binds to two Gq-coupled receptor isoforms, ETHR-A and ETHR-B, which arise from alternative splicing of a single receptor gene and are differentially expressed throughout the body (Figure 1)(Park et al., 2003). ETHR-A and ETHR-B differ substantially in their pharmacological properties and tissue expression patterns. ETHR-A exhibits higher binding affinity for ETH and is broadly expressed across central and peripheral neurons involved in ecdysis coordination and adult behaviors, while ETHR-B shows lower binding affinity and more restricted expression in specific cell populations.

During the pupal stage, these receptors are localized in the central nervous system and coordinate the specific motor patterns required to shed the cuticle during ecdysis (Kim et al., 2006). Specifically, ETH activates sequential peptidergic neuron ensembles within the central nervous system, including kinin, eclosion hormone, and crustacean cardioactive peptide (CCAP)

neurons, to orchestrate the stereotyped pre-ecdysis, ecdysis, and post-ecdysis behavioral phases (Kim et al., 2006). Despite the absence of ecdysis in adulthood, ETH receptors remain expressed across adult male tissues and contribute to a broad range of adult behaviors and processes (Figure 1). Specifically in adult females, ETHR knockdown decreases fecundity and impairs vitellogenesis (Meiselman et al., 2017). In adult male antennal lobe interneurons, ETH receptor knockdown elevates male-male courtship behavior (Deshpande et al., 2019). This effect was localized to interneurons expressing fruitless, a transcription factor that acts as a master regulator of adult male *Drosophila melanogaster* courtship behavior (Deshpande et al., 2019). In the male mushroom body γ lobe and in octopaminergic dorsal-anterior-lateral (DAL) neurons, ETH deficiency and subsequent ETH release revealed the role of ETH signaling in the formation and retention of long-term courtship memory (Lee & Adams, 2021). Particularly, the octopaminergic identity of the DAL neurons further suggests that ETH signaling regulates arousal through octopamine release, with ETH acting as an upstream endocrine signal that primes the male nervous system for courtship-relevant learning (Lee & Adams, 2021). Within the gustatory system, ETH receptors expressed in GR32A-positive bitter-sensing neurons mediate male sensitivity to male pheromones such as 7-tricosene (7-T), to promote post-copulation courtship inhibition (PCCI) (Meiselman et al., 2022). The same study identified ETHR expression on OR67D-positive olfactory neurons that detect the male pheromone 11-cis-vaccenyl acetate (cVA) and further promote PCCI (Meiselman et al., 2022). Finally, in the corpora allata, ETH drives the synthesis of juvenile hormone (JH) (Meiselman et al., 2017) and functions within an endocrine network that includes the steroid hormone 20-hydroxyecdysone (20E). Mechanistically, elevated 20E suppresses βFTZ-F1, the secretory competence factor required for ETH exocytosis, causing ETH to remain stored within Inka cell secretory vesicles. Once 20E levels fall, βFTZ-F1 levels

increase, causing Inka cells to regain secretory competence as ETH is subsequently released into the hemolymph. During both heat and nutritional stress, 20E increases, which inhibits ETH release from Inka cells (Meiselman et al., 2018).

Across these adult functions, ETH signaling has been implicated as a modulator of male courtship behavior. Adult male *Drosophila melanogaster* perform courtship through a stereotyped behavioral sequence consisting of orienting toward the female, tapping with the foreleg, producing a courtship song through wing vibration, licking the female's genitalia, attempting copulation, and ultimately achieving successful copulation (Figure 2) (Yamamoto et al., 2014). Each step in this sequence depends on sensory, motor, and motivational neural circuits, some of which have been shown to express ETH receptors. This convergence of ETH suggests that it may function as a modulator of courtship progression towards successful copulation. In addition, regulation of ETH by 20E under stress conditions suggests that ETH may itself function as a stress response molecule. I therefore hypothesize that ETH is a necessary endocrine signal regulating copulation success in adult male *Drosophila melanogaster*, and that ETH functions as a stress response molecule capable of rescuing courtship deficits produced by heat stress.

SIGNIFICANCE

The significance of my work lies in the following departures from prior approaches to studying ETH signalling in adult male *Drosophila melanogaster*. While ETH has been linked to male-male courtship interactions and to long-term courtship memory assessed after training, no study has directly examined acute male-female courtship behavior after ETH modulation (Deshpande et al., 2019; Lee & Adams, 2021). It therefore remains unknown whether ETH influences the adult male courtship sequence toward successful copulation in a heterosexual

pairing. By directly analyzing acute male-female interactions in real time, my experiment addresses this gap directly and provides the first behavioral test of ETH's role in adult reproductive success.

Second, although thermogenetic activation of Inka cells has previously been used to manipulate ETH release (Lee & Adams, 2021), no study has applied optogenetic activation to these cells. My current work utilizes CsChrimson, a red-shifted channelrhodopsin developed specifically for behavioral neuroscience in adult *Drosophila melanogaster* (Titlow et al., 2015). Compared with TRPA1-based thermogenetic tools, CsChrimson offers substantially greater temporal control and stimulation potency. Unlike TRPA1 channels, which adapt slowly and produce only transient neural activation, CsChrimson channels resist adaptation and support rapid and sustained activation (Inagaki et al., 2014). Moreover, CsChrimson benefits from red-light activation, which penetrates the adult cuticle more effectively than the shorter wavelengths required by earlier channelrhodopsins and avoids confounding activation of the visual system (Titlow et al., 2015). By applying this modern optogenetic tool to Inka cells for the first time, this study enables precise control over ETH release. Beyond the individual advantages of optogenetic activation, the parallel use of both CsChrimson and dTRPA1 within a single study provides convergent validation of ETH's role in courtship rescue through the elimination of method-specific confounding variables. In addition, both methods can be further adopted to study other peptide hormone systems and their modulation of behavior.

Third, this work modulates ETH endogenously by depolarizing Inka cells through CsChrimson or TRPA1 activation, triggering the native Ca^{2+}-dependent vesicular release of ETH. Previous studies have introduced ETH in an exogenous manner through hemolymph injection, which represents non-physiological hormone concentrations. This exogenous exposure bypasses

the natural dynamics of Inka cell ETH secretion, which obscures the true role of endogenous ETH signaling in courtship behavior. Therefore, my endogenous manipulation of Inka cells preserves both the native release mechanism and the physiological concentration range of ETH, allowing a more faithful test of its function in adult courtship behavior and stress responses.

Beyond the specific findings on courtship behavior, this work contributes to a broader understanding of how environmental stress influences behavioral output through endocrine signaling. By identifying ETH signalling as the link between stress and reproductive behavior, this study supports the broader principle that peptide hormones influence decision-making under environmental stress. Although animals continually face trade-offs between competing behavioral priorities including reproduction, foraging, predator avoidance, and rest, the regulatory mechanisms that integrate internal physiological state with external environmental conditions to drive these decisions remain an active area of investigation. Therefore, the integrative role of ETH likely reflects evolutionary pressures favoring organisms that allocate reproductive effort dynamically in response to environmental challenge, aligning with our exploration of the function of ETH circulation within adult male *Drosophila melanogaster*.

Finally, this study introduces a modern computational behavioral analysis pipeline to the Adams lab for the first time for behavior analysis. Courtship has historically been quantified by manual scoring, which is labor-intensive, susceptible to observer bias, and limited in high-throughput pattern analyses. To address these constraints, this project applies SLEAP, a deep-learning-based multi-animal pose estimation framework capable of tracking individual body parts of interacting flies (Pereira et al., 2022). The pose estimation data is then transferred into the Movement Python toolbox for downstream kinematic and trajectory analysis of the resulting pose tracks (Sirmpilatze et al., 2024). In addition, custom Python programs were

developed to define specific trends present across courtship trials. By analyzing the progression of courtship through high-resolution trajectory tracking, my experiment captures fine-grained spatial and temporal features of male behavior that have not been previously accessible through traditional methods. This includes male locomotion, pursuit dynamics, spatial co-localization with the female, courtship reset frequency, and initiation latency. Through this pipeline, new patterns and behaviors can be revealed, advancing the precision and depth at which courtship dynamics and other complex behaviors can be quantified in *Drosophila melanogaster*.

METHODS

My study tested how Inka cell activation modulates Drosophila melanogaster male courtship behavior under heat stress conditions, utilizing both optogenetic and thermogenetic approaches.

Transgenic fly generation (GAL4/UAS)

Inka cell activation was achieved using the GAL4/UAS binary expression system, a widely used genetic tool that enables cell-specific transgene expression in *Drosophila melanogaster* (Brand & Perrimon, 1993). In this system, a GAL4 driver line expresses the yeast transcription factor GAL4 under the control of a cell-specific promoter. When this driver line is crossed to a UAS responder line carrying an effector gene downstream of an Upstream Activating Sequence (UAS), GAL4 binds the UAS in the F1 progeny and drives effector expression exclusively in the cells defined by the original promoter (Figure 3).

For this study, an ETH-Gal4 driver line restricted GAL4 expression to ETH-producing Inka cells, ensuring that any downstream effector would be expressed only in those cells. Two effector lines were used to drive cellular activation: UAS-CsChrimson for optogenetic activation through red-light stimulation (Titlow et al., 2015) and UAS-dTRPA1 for thermogenetic

activation through elevated temperature (Roessingh & Stanewsky, 2017). CsChrimson is a red-shifted channelrhodopsin that opens upon red-light exposure, allowing cation influx to depolarize the target cell. dTRPA1 is a temperature-sensitive cation channel that opens above approximately 25 °C, similarly depolarizing the target cell upon heat exposure. In both cases, depolarization of Inka cells triggers Ca^{2+}-dependent vesicular release of ETH, mimicking endogenous secretion (Figure 4).

To generate experimental crosses, virgin males and females were isolated under brief CO_2 anesthesia and transferred to vials in two reciprocal combinations: ETH-Gal4 males paired with UAS-CsChrimson females, and ETH-Gal4 females paired with UAS-CsChrimson males. The same procedure was followed for the thermogenetic set, substituting UAS-dTRPA1 for UAS-CsChrimson. The resulting F1 progeny carried both the GAL4 driver and the UAS effector, enabling Inka cell-specific ETH release upon stimulation (Figure 3).

Genetic controls

Three control genotypes were maintained alongside each experimental cross to isolate the behavioral effects of Inka cell activation from any background effects of the transgenes. ETH-Gal4 control flies expressed the GAL4 transcription factor in Inka cells but lacked any UAS effector, producing GAL4 protein with no downstream consequence. UAS-CsChrimson and UAS-dTRPA1 control flies carried the silent effector construct downstream of the UAS sequence but lacked GAL4, leaving the effector transcriptionally inactive. Canton-S, a wild-type *Drosophila melanogaster* line carrying no transgenic insertions, served as the genetic background control to confirm that the transgene expression did not influence the observed behavioral results.

Treatment conditions

Two parallel experimental sets were conducted, each with matched controls and identical environmental conditions to eliminate any treatment-associated confounding variables. In the optogenetic set, ETH-Gal4>UAS-CsChrimson flies, and the corresponding controls (ETH-Gal4 alone, UAS-CsChrimson alone, and Canton-S) were fed 100 mM all-trans-retinal (ATR), the chromophore required for channelrhodopsin function, for at least 48 hours. During the experiment, the flies were exposed to one hour of pulsing LED red-light stimulation from 9:00 to 10:00 before behavioral testing, delivered through a Grass SD9 stimulator controlling a red-light LED array positioned above the courtship arena (Guo et al., 2016). Stimulation parameters were set to 16 Hz, 12 ms delay, 4 ms pulse duration, and 4 V output. In the thermogenetic set, ETH-Gal4>UAS-dTRPA1 flies and matching controls (ETH-Gal4 alone, UAS-dTRPA1 alone, and Canton-S) were exposed to 3 hours at 31 °C (7:00 to 10:00) to sufficiently to activate dTRPA1 (Lee & Adams, 2021).

Fly maintenance

Virgin flies were collected from the pupal stage and housed individually in small vials containing FlyExpress Diet D (agar 0.56%, cornmeal 6.71%, inactivated yeast 1.59%, soy flour 0.92%, corn syrup 7.0%, propionic acid 0.44%, Tegosept (methylparaben) 0.15%). Isolated rearing was used to prevent juvenile neuronal modulation, since prior exposure to rival males is known to alter adult courtship duration through circuit-level changes that emerge during early adulthood (Kim et al., 2012). Flies were maintained in an incubator at 24 °C and 60% relative humidity under a 10:00–22:00 light cycle.

Heat stress exposure and behavioral assay

Day 4–6 age-matched virgin males and Canton-S virgin females were aspirated, rather than CO_2-anesthetized, into a 14-chamber courtship arena that physically separated each pair

until the dividers were opened (Koemans et al., 2017). Females were age-matched to the males to ensure consistent sexual maturity, and Canton-S was selected as the female genotype across all experiments to provide a uniform behavioral baseline. Additionally, CO_2 anesthesia was deliberately avoided because it perturbs the neural circuits underlying courtship behavior and produces measurable courtship deficits even after extended recovery periods (Barron, 2000). Once loaded, the courtship arena was transferred to a 31 °C incubator for three hours of heat stress exposure (7:00 to 10:00), a duration and temperature consistent with prior protocols for elevating 20E in *Drosophila melanogaster* (Meiselman et al., 2018). Following heat stress, the courtship arena was transferred to a recording room maintained at 22 °C, and behavior was recorded for ten minutes beginning at 10:10 with the removal of the chamber divider. This timing was chosen to align with the *Drosophila melanogaster* mating rhythm peak at lights-on, when innate mating drive is highest (Guo et al., 2016). Behavioral recordings were captured at 30 frames per second in 1080p resolution using a Sony Handycam HDR-CX405 camcorder positioned directly above the courtship arena. Video files were stored in a standardized format and resolution for downstream analysis. After each trial, flies were aspirated out of the chamber, which was then cleaned with 70% ethanol and dried with forced air to remove residual pheromones from prior trials.

Behavioral analysis

Video recordings were analyzed through various methods. Courtship Index (CI), defined as the proportion of observation time during which the male engaged in any courtship behavior, was calculated for each pair. Additional observations included initial courtship attempt latency and successful copulation latency. Abnormal courtship behaviors, such as freezing, extensive

grooming, female-initiated contact, and bilateral wing extensions, were additionally noted for subsequent pattern analyses.

Further behavior analysis was conducted according to the following pipeline. Each courtship chamber was cropped to cover just the circular arena and trimmed to the 10-minute period or the time of successful copulation. This video was analyzed within SLEAP through my custom-trained centroid model that tracks the head of both male and female flies (Pereira et al., 2022). Pose tracks generated by SLEAP were imported into the Movement Python toolbox (Sirmpilatze et al., 2024) for downstream kinematic analysis. Speed and trajectory plots were produced for both males and females. In addition, I developed a custom Python program that defines a spatial zone around the female and tracks male movements relative to this zone. A zone creation event is registered whenever the male enters the female's proximity, capturing the spatial co-localization that defines a courtship attempt. Zone duration measures how long the male sustains proximity within each attempt before disengaging and valid zones depend on this measurement as a threshold of differentiating between transient detection events from continuous engagement.

Statistical Analyses

All statistical analyses were performed in GraphPad Prism version 10. Sample sizes for each experimental group were determined a priori through power analysis ($\alpha = 0.9$), which established a target of $n = 18$ per group. Due to inherent variability in Drosophila melanogaster behavioral data, normal distribution was not assumed across statistical tests, and non-parametric tests were applied accordingly. Courtship Index, time to courtship initiation, and initial speed were compared across genotypes using the Kruskal-Wallis test followed by Dunn's multiple comparisons. Number of zone creations, average zone duration, and time to first zone creation

were compared between ETH-rescue and pooled control males using the Mann-Whitney U test. Successful copulation rates were analyzed as binary outcomes using pairwise two-sided Fisher's exact tests with Holm-Šídák correction for multiple comparisons. Percent mated curves were compared using the log-rank (Mantel-Cox) test for survival-style data. Differences were considered statistically significant at $p < 0.05$. Data are presented as mean ± SEM, and sample sizes for each experimental condition are reported in the corresponding figure legends.

RESULTS

Courtship Outcomes

Across both optogenetic and thermogenetic activation paradigms, courtship index (CI) differed significantly between the experimental cross and some, but not all, of the genetic controls (Figures 5A and 5B). In both cases, the experimental crosses display higher courtship indices than at least one genetic control, indicating greater overall time spent courting . Importantly, CI is a time-aggregated measure that captures the overall motivational drive to court but does not capture the temporal structure, sequencing, or fidelity of the individual behavioral elements. Thus, while this superficial analysis suggests that Inka cell activation broadly preserves or modestly enhances overall courtship engagement, it does not distinguish whether ETH release modulates specific courtship behaviors and outcomes.

Therefore, I next examined copulation success, defined as the proportion of pairings in which the male achieved successful genital coupling within the observation window, which represents the terminal outcome of the courtship sequence. Successful copulation is routinely observed in unmanipulated, age-matched pairs of 4–6 day-old wild-type flies in the absence of heat stress, and therefore serves as a basic indicator of successful courtship behavior sequence progression. In both the optogenetic and thermogenetic methods, the experimental cross

achieved a markedly higher copulation success rate than the parental and wild-type controls that was significantly significant for most comparisons (Figures 6A and 6B). Although one pairwise comparison in the optogenetic method narrowly missed the conventional $\alpha = 0.05$ threshold, a consistent pattern of significance across the remaining comparisons across both experiments was observed. With the well-documented behavioral variability inherent to *Drosophila melanogaster* male courtship, I can conclude that the single near-threshold result reflects random variation rather than a true biological difference. Taken together, these copulation success data demonstrate that Inka cell activation, and the resulting release of ETH, is sufficient to enhance the terminal outcome of the courtship sequence beyond the levels achieved by genetic controls under heat-stress conditions.

Courtship Temporal Dynamics

To evaluate the temporal trajectory by which males achieved successful copulation, I measured the cumulative percent of pairs mated as a function of time elapsed from female introduction. Across both methods, ETH-rescue males not only achieved a higher final copulation rate, as established above, but also reached that rate substantially faster than all genetic controls (Figures 7A and 7B). The convergence of this suggests that ETH release does not merely increase the probability of copulation but also accelerates the male's progression through the upstream courtship sequence, orienting, tapping, singing, licking, attempted copulation, and successful copulation. During heat stress, Inka cell activation appears to decrease the temporal window required to execute successful courtship behaviors, perhaps by the following factors: enhancing motivational drive, sensory functions, or motor functions.

To determine whether the accelerated copulation trajectory described above reflects faster initiation of courtship, I measured the latency from female introduction to the first observable

courtship behavior (male orientation toward the female). Across both methods, ETH-rescue males began courting markedly sooner than genetic controls (Figures 8A and 8B). The single non-significant comparison within the thermogenetic experiment can be also be interpreted as behavioral variability rather than a genuine absence of effect. The faster initiation observed in ETH-rescue males directly aligns with faster copulation success and may be driven by similar factors mentioned above through Inka cell activation.

To further analyze these temporal accelerations of courtship behavior, I explored whether a trend occured within the male's initial locomotor speed during the first 60 seconds following female introduction. Interestingly, genetic controls across both methods displayed opposite motor phenotypes following heat stress, while the experimental cross consistently occupied an intermediate range (Figures 9A and 9B). The ETH-Gal4/+ males displayed a high-speed phenotype, consistent with a flight-like response to heat stress, whereas UAS-CsChrimson/+ males and Canton-S males displayed a low-speed phenotype, consistent with a freeze-like response (Figures 9A and 9B). Taken together, these data suggest that heat stress elicits two opposing motor responses (flight or freeze) and that Inka cell activation normalizes these extreme phenotypes toward an intermediate state more compatible with the execution of successful courtship behavior. The single non-significant comparison in the optogenetic paradigm is again interpreted as reflecting natural behavioral variability rather than a true absence of effect. I additionally note that initial speed was quantified by automated AI-based tracking, and some between-trial variability in this measure may reflect technical differences in recording conditions rather than true biological variation.

Courtship spatial dynamics

To complement the temporal analysis presented above with a spatial analysis, I performed automated trajectory tracking of both males and females across the 600-second observation window. Analysis of these trajectories revealed three qualitatively distinct behavioral outcomes (1-3) and motivated a downstream zone-based quantification that distinguishes two separable male-side courtship deficits, which I termed Unknown Factor X and Unknown Factor Y.

Detailed analysis and pattern recognition of representative male and female trajectory plots revealed the following 3 outcomes that were seen in high frequencies across both activation methods. Outcome 1 was observed predominantly in ETH-Gal4>UAS-CsChrimson and ETH-Gal4>UAS-dTRPA1 experimental males (Figures 10A and 10B). In this outcome, the male engaged in broad chamber exploration with directed pursuit of the female during the first 150 seconds, after which both male and female trajectories converged into a tightly clustered region of the chamber during the 150–300 second window, indicating sustained spatial co-localization that culminated in successful copulation (Figures 10A and 10B). Outcome 2 was observed predominantly in genetic control males that achieved sustained locomotion but failed to copulate (Figures 11A and 11B). In this outcome, the male's trajectory remained broadly distributed across the chamber throughout all four 150-second windows, and the corresponding speed-versus-time trace exhibited multiple high-amplitude spikes reflecting repeated initiation, partial execution, and disengagement cycles (Figures 11A and 11B). This pattern directly translates to instances in which the male approached the female, began courtship, and then aborted before achieving copulation. Outcome 3 was observed in a separate subset of genetic control males in which trajectories were sparse and largely confined to peripheral regions of the chamber, with the corresponding speed traces displaying only a few isolated high-velocity events

and prolonged intervals at near-zero speed (Figures 12A and 12B). In this outcome, the male failed to localize to or approach the female within the observation window, precluding any opportunity for copulation.

To convert these qualitative trajectory observations into quantitative measures, I defined courtship-relevant proximity zones around the female and quantified two complementary metrics: the number of zone creations (the number of discrete entries the male made into a courtship-relevant zone over the 600-second observation window) and the time to first zone creation (the latency from chamber loading to the male's first such entry). These two metrics target the two failure outcomes described above: zone creations with Outcome 2, while time to first zone creation with Outcome 3. ETH-rescue males across both methods produced significantly fewer zone creations than pooled genetic control males within Outcome 2 (Figure 13). The substantially elevated zone creation count in control males reflects the repeated resetting cycles characteristic of Outcome 2, which I believe is driven by Unknown Factor X. Additionally, ETH-rescue males across both methods entered female proximity significantly faster than pooled genetic control males within Outcome 3. This high latency observed in genetic control males reflects the failure to localize to and approach the female characteristic of Outcome 3, which I believe is driven by Unknown Factor Y.

A critical alternative interpretation of the male-side deficits described above is that copulation failure in control pairs reflects reduced female receptivity rather than a male behavioral defect. To rule out this possibility, I measured average zone duration, defined as the average time the female remained within courtship-relevant proximity per male zone entry. This metric serves as a proxy for female receptivity: receptive females remain near the courting male, while unreceptive females rapidly disengage. Average zone duration did not differ significantly

between cross and pooled genetic control pairs across both methods, indicating that female receptivity remained comparable across all treatment groups (Figure 15). The preservation of normal female receptivity confirms that the copulation deficits observed in genetic controls are driven by male-side abnormalities, through Unknown Factors X and Y.

DISCUSSION

Heat stress produces courtship deficits that are rescued by Inka cell activation.

The present findings demonstrate that three hours of heat stress at 31 °C produces a reproducible set of courtship deficits in adult male *Drosophila melanogaster*. Genetic controls across both experiments showed that heat stressed males experienced decreased copulation success, increased copulation latency, and increased time to courtship initiation. ETH-Gal4 control males exhibited elevated initial speeds, representing a flight-like response to the heat stress. On the other hand, UAS-CsChrimson, UAS-TRPA1, and Canton-S control males exhibited decreased initial speeds, representing a freeze-like response to the heat stress. Direct optogenetic and thermogenetic activation of Inka cells significantly attenuated each of the courtship deficits produced by heat stress. ETH-rescue males across both experiments experienced increased copulation success, decreased copulation latency, and decreased time to courtship initiation. In addition, ETH-rescue males exhibited intermediate initial speeds relative to the high and low initial speeds present across control males.

Trajectory analysis reveals Unknown Factor X- and Y-driven courtship deficits

The post-hoc trajectory analysis revealed three central courtship outcomes that occurred reproducibly across both experiments. Outcome 1 was seen in ETH-rescue males and is characterized by early male pursuit followed by spatial co-localization with the female and successful copulation. Outcome 2 was seen in genetic controls and is characterized by repeated

resetting, temporary localization, and disengagement. Outcome 3 was seen in genetic controls and is characterized by failure of courtship initiation and low movement. When comparing Outcomes 1 and 2, control males in Outcome 2 produced significantly more zone creations than ETH-rescue males, reflecting the repeated resetting characteristic of Unknown Factor X. When comparing Outcomes 1 and 3, control males in Outcome 3 showed prolonged time to first zone creation, revealing Unknown Factor Y. The preservation of female receptivity across all experiments, evidenced by constant average zone durations between Cross and control pairs, supports the conclusion that these courtship deficits are male-driven through Unknown Factors X and Y.

There are several mechanisms that could explain the repeat resetting phenotype driven by Unknown Factor X, which occurs during the active phase of male courtship behavior. First, ETH may support normal courtship song production via ETHR expression on song-producing motor neurons, P1 command neurons, or intermediate song circuits, such that ETH deficiency disrupts song parameters and prompts female rejection (Yamamoto et al., 2014). Second, ETH may support male orientation toward the female via ETHR expression on motor neurons coordinating turning behavior or on visual processing circuits, such that ETH deficiency disrupts spatial alignment and triggers repeated disengagement. Third, ETH may support central coordination of the courtship behavioral program, such that ETH deficiency causes males to execute courtship steps in incorrect order or with insufficient intensity, prompting female rejection.

On the other hand, there are several other mechanisms that could explain the courtship initiation failure phenotype driven by Unknown Factor Y. First, ETH may modulate the detection of female pheromones via ETHR expression on chemosensory neurons, such that ETH deficiency could impair the male's ability to detect the chemosensory cues that normally trigger

courtship initiation. Second, ETH may support internal mating drive via ETHR expression on P1 command neurons or on circuits regulating P1 excitability, such that ETH deficiency lowers the threshold for courtship initiation and decreases mating drive. Third, ETH may support visual tracking of the female via ETHR expression on visual sensory neurons or downstream processing circuits, such that ETH deficiency impairs the male's ability to localize and approach the females.

Limitations

Several limitations within my study must be considered. First, direct biochemical measurement of circulating ETH was not performed in this study, so the conclusion that Inka cell activation increases ETH release is inferred from the behavioral rescue rather than confirmed quantitatively. Second, the optogenetic and thermogenetic activation periods differ in duration, with CsChrimson activated through one hour of red-light exposure and dTRPA1 activated throughout the full three-hour heat-stress window. While both methods produced comparable behavioral rescue, this difference in activation duration means that the experiments are not perfectly matched in terms of total ETH release, and a dynamic study of ETH release with each method is necessary. Third, females in all experimental pairs were exposed to the same three-hour heat stress as the males, which could have decreased circulating ETH and influenced their behavior. Fourth, a subset of recordings with degraded camera conditions produced low-confidence pose estimation outputs and were excluded from trajectory and zone-based analyses, reducing usable sample sizes for those metrics. Finally, manual scoring of Courtship Index was performed non-blind to genotype, which introduces the potential for observer bias and may have produced variability in the CI measurements.

CURRENT WORK AND FUTURE DIRECTIONS

Current work

Three follow-up experiments are currently underway to extend the findings of the present study. The first is a βFTZ-F1 RNAi courtship experiment, which targets the secretory competence factor required for ETH release from Inka cells. By knocking down βFTZ-F1 expression, this experiment produces a functional ETH deficiency without altering the ETH gene itself, providing an independent line of evidence for ETH's role in acute courtship behavior. If βFTZ-F1 RNAi males experience similar courtship deficits observed in heat-stressed control males, the conclusion that ETH ensures copulation success and decreases heat-stressed courtship deficits will be substantially strengthened.

The second ongoing experiment is a Y-maze pheromone preference assay designed to test whether ETH-deficient males show reduced sensitivity to female pheromones, directly addressing the chemosensory hypothesis raised for Unknown Factor Y. Practice trials are currently underway to refine the assay protocol, eliminate observer biases, and control for confounding environmental variables before formal data collection begins. If ETH-deficient males show diminished pheromone preference in the Y-maze, the chemosensory mechanism for Unknown Factor Y will gain direct experimental support.

A third experiment currently in development extends the present study to a cellular characterization of CsChrimson function in Inka cells. To enable direct visualization of channel expression, ETH-Gal4>UAS-CsChrimson F1 progeny were generated using a UAS-CsChrimson construct carrying a YFP (mVenus) tag, allowing identification of CsChrimson-expressing Inka cells through fluorescence microscopy following dissection. This visualization approach also enables investigation of how UAS copy number influences transgene expression, with twenty

UAS sites present in this construct, providing an opportunity to characterize how multi-copy UAS arrangements affect channelrhodopsin expression density and downstream activation potency. After identifying CsChrimson-positive Inka cells along the tracheal system at their most accessible points, individual Inka cells will be dissected and mounted on slides for live-cell imaging. Calcium dynamics will be measured using Calbryte, a calcium-sensitive fluorescent indicator, to quantify cellular responses under varying red-light stimulation parameters. By systematically varying pulse frequency, pulse duration, and total illumination time, this experiment aims to identify optimal stimulation parameters for maximal ETH release and to characterize CsChrimson desensitization under prolonged red-light exposure, an aspect of CsChrimson function in Inka cells that has not been previously addressed.

Future Work

Several additional experiments are planned to extend this work. First, fluorescence-based mapping of ETH receptor isoforms ETHR-A and ETHR-B will be performed to identify the specific neuronal populations expressing each isoform in adult tissues. Crosses generating reporter expression in candidate cell types, including chemosensory neurons, P1 command neurons, and song-producing motor neurons, will explore the mechanisms underlying Unknown Factors X and Y. Second, hemolymph ETH measurements will be performed to directly quantify circulating ETH in heat-stressed control males compared to ETH-rescue males. Pressurized hemolymph extraction followed by ELISA will provide biochemical confirmation that the optogenetic and thermogenetic manipulations produce the intended endocrine effect. Third, the courtship song will be recorded directly using a microphone embedded within the courtship arena, allowing acoustic analysis of song parameters in heat-stressed control males and ETH-rescue males. Further analysis of song onset, type, duration, and sequence will test the

courtship song hypothesis raised for Unknown Factor X and determine whether ETH signaling supports specific components of song production. Finally, juvenile hormone (JH) deficiency courtship experiments will extend the analysis downstream of ETH. I would expect JH-deficient males to experience similar courtship deficits seen with heat-stressed males based on our knowledge of the endocrine network.

CONCLUSION

The present study establishes ETH as an essential endocrine component of acute adult male *Drosophila melanogaster* copulation success and as a stress response molecule whose release rescues heat-stress-induced courtship deficits. Direct activation of Inka cells through both optogenetic CsChrimson stimulation and thermogenetic dTRPA1 stimulation produced similar rescue effects across all measured behavioral metrics, including increased copulation success, faster courtship initiation, normalized initial speeds, and reduced courtship resetting. The corroborating results validate both optogenetic and thermogenetic approaches as effective tools for manipulating Inka cell activity in adult behavioral studies. The heat-stress exposure produced the Outcome 2 and Outcome 3 patterns, which were resolved into the Outcome 1 pattern through Inka cell activation, further suggesting that ETH signaling may act through parallel pathways influencing both the initiation of courtship and its successful execution. Methodologically, this work also introduces a modern computational behavioral analysis pipeline to the lab, integrating SLEAP-based pose estimation, the movement Python toolbox, and custom zone-occupancy programs to quantify courtship behavior at higher spatial and temporal resolution than manual scoring permits. This pipeline establishes an analytical framework that can be adopted by future projects investigating fine-scale behavioral patterns. This work further contributes towards our understanding of the function of ETH within adult male *Drosophila melanogaster*.

REFERENCES

Barron, A. B. (2000). Anaesthetising Drosophila for behavioural studies. Journal of Insect Physiology, 46(4), 439–442. https://doi.org/10.1016/S0022-1910(99)00129-8

Brand, A. H., & Perrimon, N. (1993). Targeted gene expression as a means of altering cell fates and generating dominant phenotypes. Development, 118(2), 401–415. https://doi.org/10.1242/dev.118.2.401

Deshpande, S. A., Meiselman, M., Hice, R. H., Arensburger, P., Rivera-Perez, C., Kim, D.-H., Croft, R. L., Noriega, F. G., & Adams, M. E. (2019). Ecdysis triggering hormone receptors regulate male courtship behavior via antennal lobe interneurons in Drosophila. General and Comparative Endocrinology, 278, 79–88. https://doi.org/10.1016/j.ygcen.2018.12.003

Guo, F., Yu, J., Jung, H. J., Abruzzi, K. C., Luo, W., Griffith, L. C., & Rosbash, M. (2016). Circadian neuron feedback controls the Drosophila sleep–activity profile. Nature, 536(7616), 292–297. https://doi.org/10.1038/nature19097

Inagaki, H. K., Jung, Y., Hoopfer, E. D., Wong, A. M., Mishra, N., Lin, J. Y., Tsien, R. Y., & Anderson, D. J. (2014). Optogenetic control of Drosophila using a red-shifted channelrhodopsin reveals experience-dependent influences on courtship. Nature Methods, 11(3), 325–332. https://doi.org/10.1038/nmeth.2765

Kim, W. J., Jan, L. Y., & Jan, Y. N. (2012). Contribution of visual and circadian neural circuits to memory for prolonged mating induced by rivals. Nature Neuroscience, 15(6), 876–883. https://doi.org/10.1038/nn.3104

Kim, Y.-J., Žitňan, D., Galizia, C. G., Cho, K.-H., & Adams, M. E. (2006). A command chemical triggers an innate behavior by sequential activation of multiple peptidergic ensembles. Current Biology, 16(14), 1395–1407. https://doi.org/10.1016/j.cub.2006.06.027

Koemans, T. S., Oppitz, C., Donders, R. A. T., van Bokhoven, H., Schenck, A., Keleman, K., & Kramer, J. M. (2017). Drosophila courtship conditioning as a measure of learning and memory. Journal of Visualized Experiments, (124), 55808. https://doi.org/10.3791/55808

Lee, S.-S., & Adams, M. E. (2021). Regulation of Drosophila long-term courtship memory by ecdysis triggering hormone. Frontiers in Neuroscience, 15, 670322. https://doi.org/10.3389/fnins.2021.670322

Meiselman, M., Lee, S.-S., Tran, R.-T., Dai, H., Ding, Y., Rivera-Perez, C., Wijesekera, T. P., Dauwalder, B., Noriega, F. G., & Adams, M. E. (2017). Endocrine network essential for reproductive success in Drosophila melanogaster. Proceedings of the National Academy of Sciences, 114(19), E3849–E3858. https://doi.org/10.1073/pnas.1620760114

Meiselman, M. R., Kingan, T. G., & Adams, M. E. (2018). Stress-induced reproductive arrest in Drosophila occurs through ETH deficiency-mediated suppression of oogenesis and ovulation. BMC Biology, 16(1), 18. https://doi.org/10.1186/s12915-018-0484-9

Meiselman, M. R., Ganguly, A., Dahanukar, A., & Adams, M. E. (2022). Endocrine modulation of primary chemosensory neurons regulates Drosophila courtship behavior. PLOS Genetics, 18(8), e1010357. https://doi.org/10.1371/journal.pgen.1010357

Park, Y., Žitňan, D., Gill, S. S., & Adams, M. E. (1999). Molecular cloning and biological activity of ecdysis-triggering hormones in Drosophila melanogaster. FEBS Letters, 463(1–2), 133–138. https://doi.org/10.1016/S0014-5793(99)01622-1

Park, Y., Filippov, V., Gill, S. S., & Adams, M. E. (2002). Deletion of the ecdysis-triggering hormone gene leads to lethal ecdysis deficiency. Development, 129(2), 493–503. https://doi.org/10.1242/dev.129.2.493

Park, Y., Kim, Y.-J., Dupriez, V., and Adams, M. E., (2003). Two subtypes of ecdysis-triggering hormone receptor in Drosophila melanogaster. Journal of Biological Chemistry, 278(20), 17710–17715. https://doi.org/10.1074/jbc.M301119200

Pereira, T. D., Tabris, N., Matsliah, A., Turner, D. M., Li, J., Ravindranath, S., Papadoyannis, E. S., Normand, E., Deutsch, D. S., Wang, Z. Y., McKenzie-Smith, G. C., Mitelut, C. C., Castro, M. D., D'Uva, J., Kislin, M., Sanes, D. H., Kocher, S. D., Wang, S. S.-H., Falkner, A. L., Shaevitz, J. W., & Murthy, M. (2022). SLEAP: A deep learning system for multi-animal pose tracking. Nature Methods, 19(4), 486–495. https://doi.org/10.1038/s41592-022-01426-1

Roessingh, S., & Stanewsky, R. (2017). The Drosophila TRPA1 channel and neuronal circuits controlling rhythmic behaviours and sleep in response to environmental temperature. International Journal of Molecular Sciences, 18(10), 2028. https://doi.org/10.3390/ijms18102028

Sirmpilatze, N., Lo, C. H., Miñano, S., Peri, B. D., Sharma, D., Porta, L., Varela, I., & Tyson, A. L. (2024). movement: A Python toolbox for analysing animal body movements across space and time [Computer software]. Zenodo. https://doi.org/10.5281/zenodo.12755724

Titlow, J. S., Johnson, B. R., & Pulver, S. R. (2015). Light activated escape circuits: A behavior and neurophysiology lab module using Drosophila optogenetics. Journal of Undergraduate Neuroscience Education, 13(3), A166–A173.

Yamamoto, D., Sato, K., & Koganezawa, M. (2014). Neuroethology of male courtship in Drosophila: from the gene to behavior. Journal of Comparative Physiology A, 200(4), 251–264. https://doi.org/10.1007/s00359-014-0891-5

FIGURES

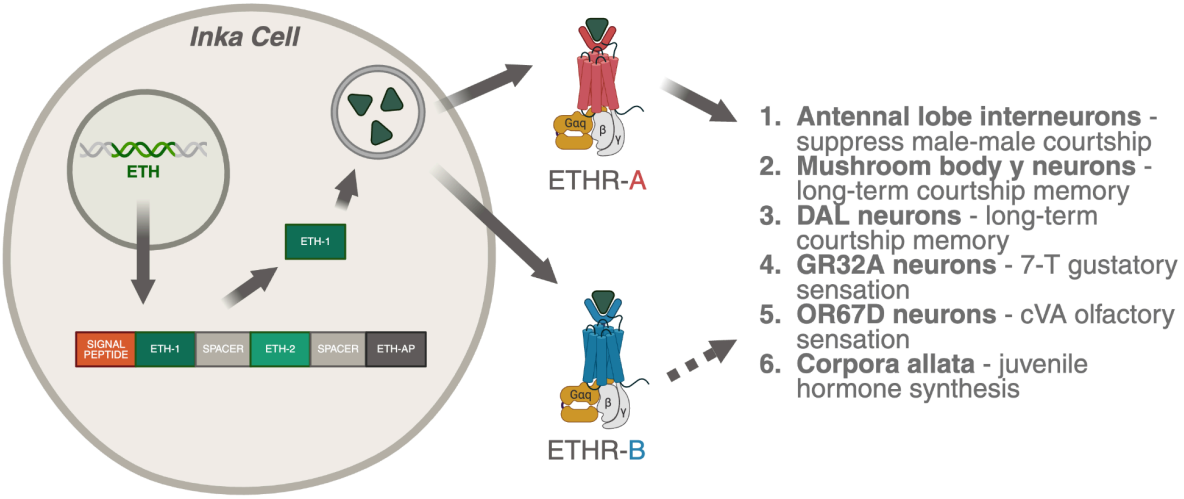


Figure 1. Ecdysis Triggering Hormone (ETH) processing in Inka cells and ETH receptor (ETHR) signaling to adult male target tissues. Within the Inka cell (left), the ETH gene is transcribed in the nucleus and translated into a precursor polypeptide (bottom) consisting of an N-terminal signal peptide, ETH-1 and ETH-2 separated by spacer sequences, and a C-terminal associated peptide (ETH-AP). Following proteolytic processing, the ETH-1 is packaged into secretory vesicles and released into the hemolymph. Once secreted, ETH-1 binds to both ETHR-A and ETHR-B, two Gq protein–coupled receptors. Major ETHR-A signaling (solid arrows) and minor ETHR-B signaling (dashed arrows) operate in six identified target populations that regulate male reproductive behavior, memory, sensory function, and endocrine output.

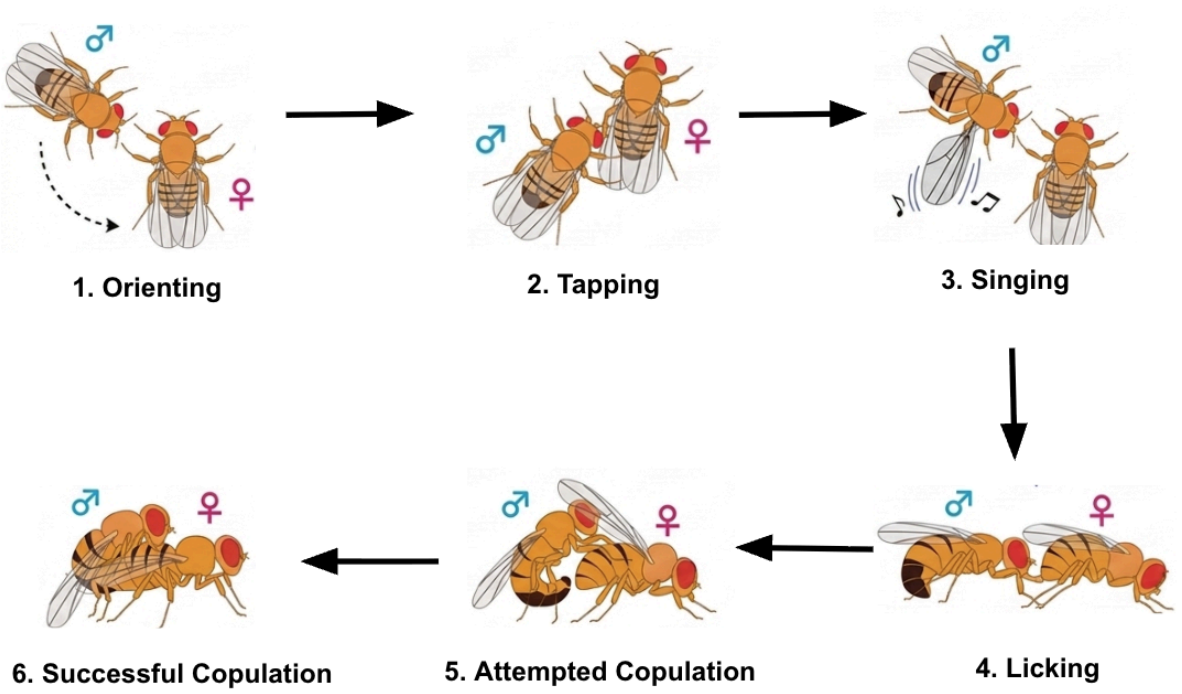


Figure 2. The stereotyped sequence of *Drosophila melanogaster* male courtship behavior. Adult male courtship in *Drosophila melanogaster* unfolds as a highly stereotyped and sequential process composed of behavioral elements that further enable successful copulation: (1) Orienting, in which the male turns toward and aligns his body axis with the female using primarily visual cues; (2) Tapping, in which the male contacts the female's abdomen with his foreleg tarsi to sample non-volatile cuticular hydrocarbons via gustatory receptor neurons; (3) Singing, in which the male extends and vibrates one wing to produce a species-specific courtship song composed of alternating sine and pulse components; (4) Licking, in which the male extends his proboscis to contact the female's ovipositor for additional close-range gustatory sampling; (5) Attempted copulation, in which the male curls his abdomen ventrally and attempts to mount the female; and (6) Successful copulation, in which genital coupling is achieved and the pair remains in copulation position for approximately 15–20 minutes. Adapted from Yamamoto, Sato, & Koganezawa (2014).

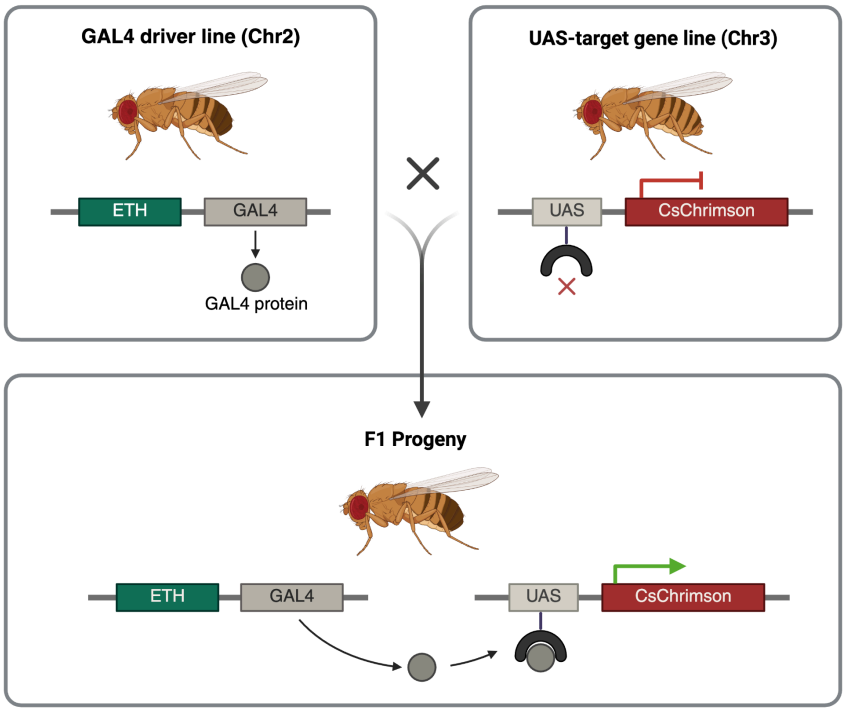


Figure 3. Generation of ETH-Gal4>UAS-CsChrimson F1 progeny via the GAL4/UAS binary expression system. Schematic illustrating the bipartite GAL4/UAS system used to drive cell specific expression of the red-shifted channelrhodopsin CsChrimson in ETH-producing Inka cells. The parental driver line (top left) carries a transgene on chromosome 2 in which the ETH promoter directs expression of the yeast transcription factor GAL4, producing GAL4 protein in all ETH-expressing cells (Inka cells). The parental responder line (top right) carries a transgene on chromosome 3 in which the CsChrimson coding sequence is placed downstream of the Upstream Activating Sequence (UAS); in the absence of GAL4, this transgene remains transcriptionally silent. Crossing the two parental lines yields F1 progeny (bottom) that inherit both transgenes. In these offspring, GAL4 protein produced under control of the ETH promoter binds to the UAS element and activates transcription of CsChrimson exclusively in Inka cells, enabling optogenetic activation of these cells upon exposure to red light.

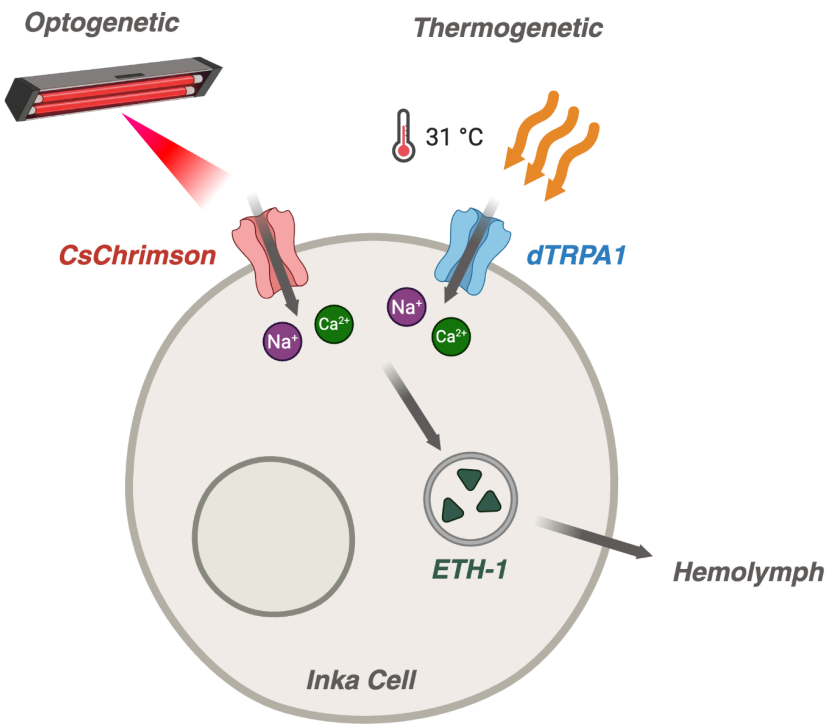


Figure 4. Optogenetic and thermogenetic activation of Inka cells triggers ETH-1 release. Schematic depicting two complementary genetic strategies used to selectively activate Inka cells and stimulate ETH-1 release into the hemolymph. In the optogenetic approach (left), Inka cells express the red-shifted channelrhodopsin CsChrimson under GAL4/UAS control; illumination with red light for 1 hour opens the channel and drives an inward flux of Na^+ and Ca^{2+} that depolarizes the cell. In the thermogenetic approach (right), Inka cells instead express the dTRPA1, a heat-activated cation channel that opens at 31 °C and similarly produces a depolarizing Na^+ and Ca^{2+} influx. In both cases, the resulting rise in intracellular Ca^{2+} triggers fusion of ETH-1–containing secretory vesicles with the plasma membrane, releasing mature ETH-1 peptide into the hemolymph where it can act on ETHR-expressing target tissues throughout the adult male.

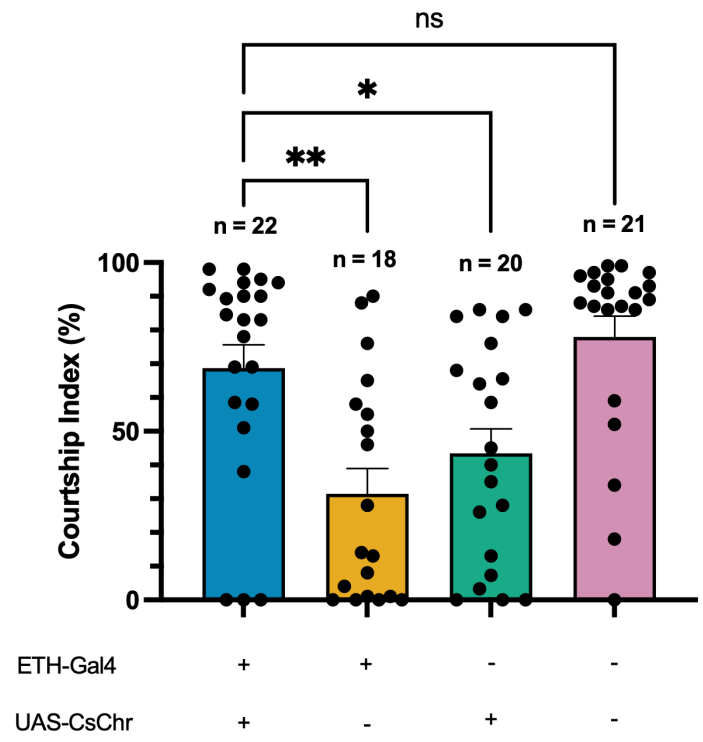


Figure 5A. Optogenetic activation of Inka Cells during heat stress yields comparable CI to wild-type males. After a 3-hour heat-stress period during which Inka cells were optogenetically activated in the final hour, male courtship index was increased in both ETH-Gal4>UAS-CsChrimson and Canton-S males relative to genetic controls. Blue, ETH-Gal4>UAS-CsChrimson (n=22); Yellow, ETH-Gal4/ETH-Gal4 (n=18); Green, UAS-CsChrimson/UAS-CsChrimson (n=20); Pink, Canton-S/Canton-S (n=21). Bars show mean ± SEM. Statistics: Kruskal–Wallis test across groups followed by Dunn's multiple comparisons; ns $p>0.05$, * $p<0.05$, ** $p<0.01$.

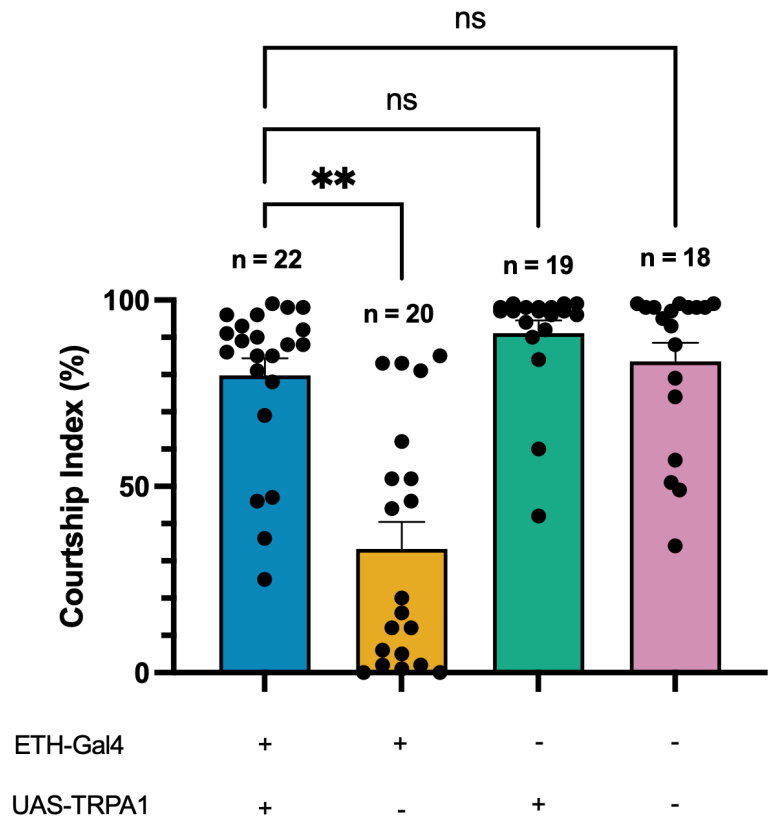


Figure 5B. Thermogenetic activation of Inka Cells during heat stress yields comparable CI to wild-type males. After a 3-hour heat-stress period during which Inka cells were thermogenetically activated in the final hour, male courtship index was increased in ETH-Gal4>UAS-TRPA1, UAS-TRPA1, and Canton-S males relative to ETH-Gal4. Blue, ETH-Gal4>UAS-TRPA1 (n=22); Yellow, ETH-Gal4/ETH-Gal4 (n=20); Green, UAS-TRPA1/UAS-TRPA1 (n=19); Pink, Canton-S/Canton-S (n=18). Bars show mean ± SEM. Statistics: Kruskal–Wallis test across groups followed by Dunn's multiple comparisons; ns $p>0.05$, ** $p<0.01$.

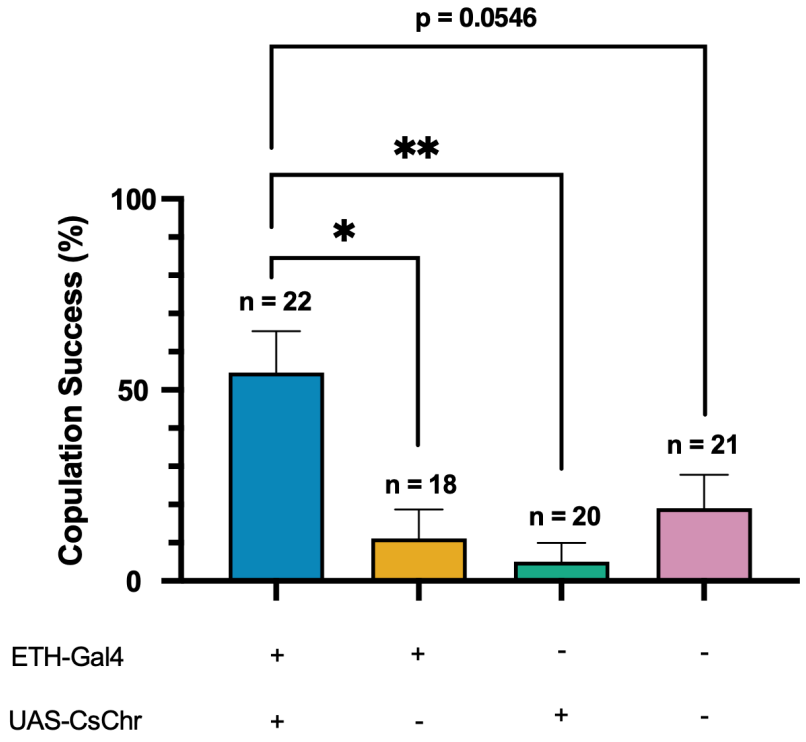


Fig 6A. Optogenetic activation of Inka cells during heat stress exposure increases copulation success. After a 3-hour heat-stress period during which Inka cells were optogenetically activated in the final hour, male copulation success increased in ETH-Gal4>UAS-CsChrimson relative to genetic controls. Blue, ETH-Gal4>UAS-CsChrimson (n=22); yellow, ETH-Gal4/ETH-Gal4 (n=18); green, UAS-CsChrimson/UAS-CsChrimson (n=20); pink, Canton-S/Canton-S (n=21). Bars show mean ± SEM. Statistics: pairwise two-sided Fisher's exact tests with Holm-Šídák correction for multiple comparisons; ns $p>0.05$, * $p<0.05$, ** $p<0.01$.

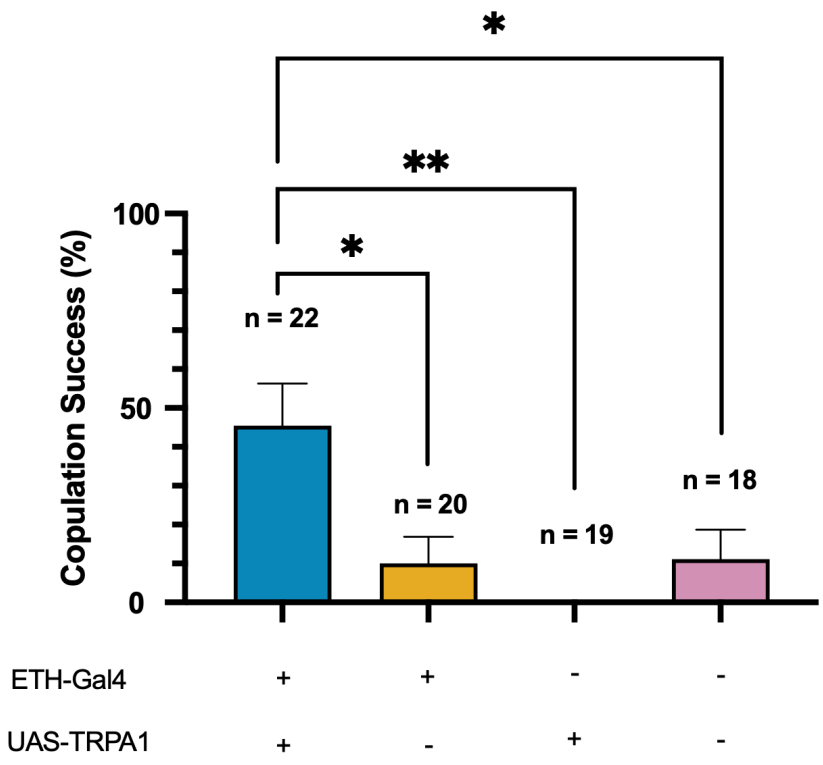


Fig 6B. Thermogenetic activation of Inka cells during heat stress increases copulation success. After a 3-hour heat-stress period during which Inka cells were thermogenetically activated in the final hour, male copulation success increased in ETH-Gal4>UAS-TRPA1 relative to genetic controls. Blue, ETH-Gal4>UAS-TRPA1 (n=22); yellow, ETH-Gal4/ETH-Gal4 (n=20); green, UAS-TRPA1/UAS-TRPA1 (n=19); pink, Canton-S/Canton-S (n=18). Bars show mean ± SEM. Statistics: pairwise two-sided Fisher's exact tests with Holm-Šídák correction for multiple comparisons; * $p<0.05$, ** $p<0.01$.

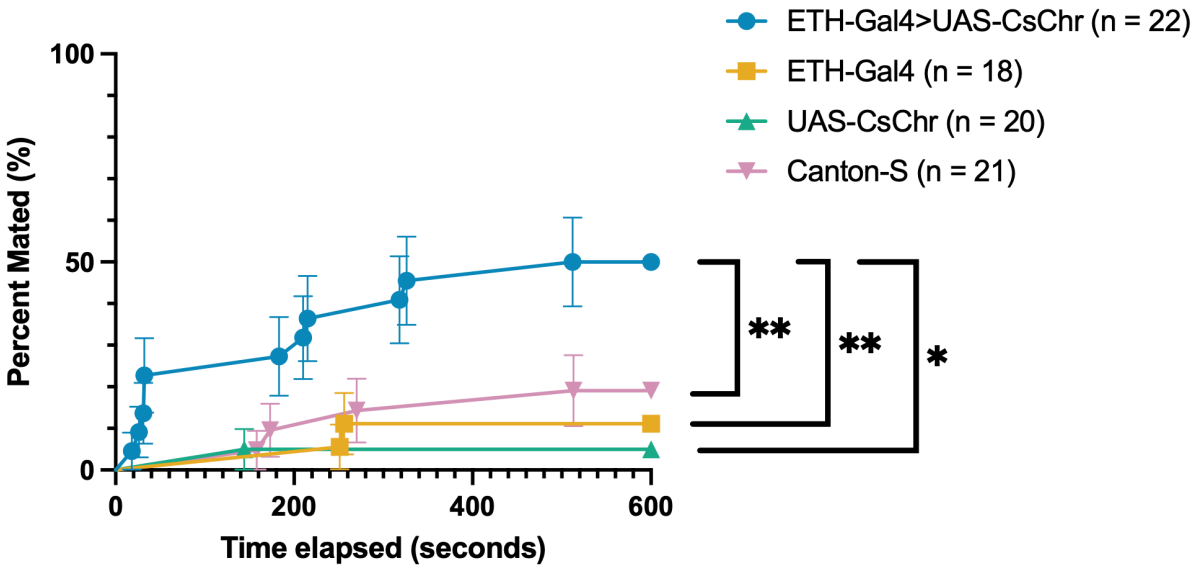


Fig 7A. Optogenetic activation of Inka cells during heat stress accelerates copulation success. After a 3-hour heat-stress period during which Inka cells were optogenetically activated in the final hour, the time to successful copulation shortened in ETH-Gal4>UAS-CsChrimson relative to genetic controls. Blue, ETH-GAL4>UAS-CsChrimson (n=22); Yellow, ETH-GAL4/ETH-GAL4 (n=18); Green, UAS-CsChrimson/UAS-CsChrimson (n=20); Pink, Canton-S/Canton-S (n=21). Points show time to successful copulation events ± SE. Statistics: Pairwise comparisons used the log-rank (Mantel–Cox) test. Significance thresholds:; * $p<0.05$, ** $p < 0.01$.

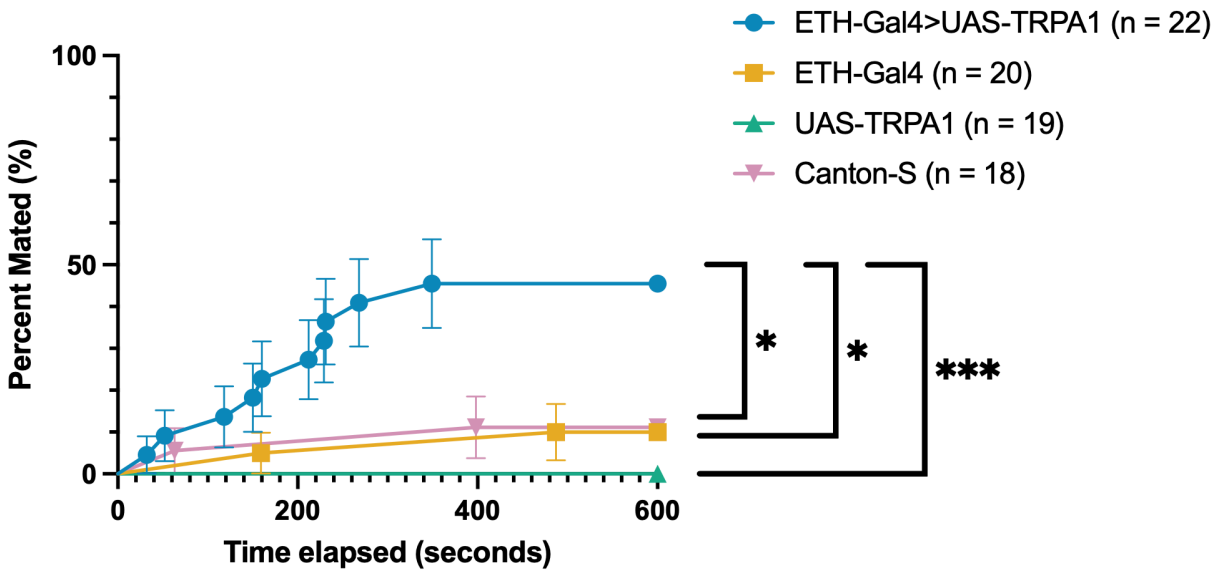
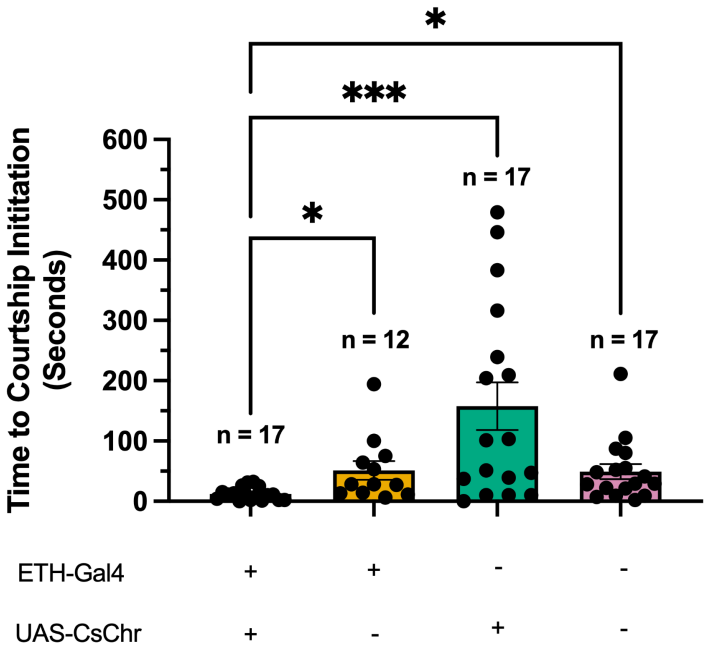
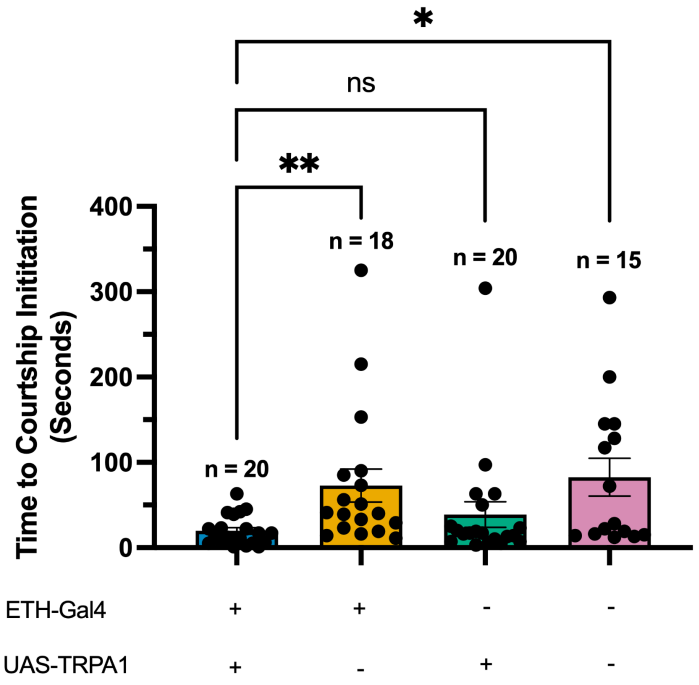


Fig 7B. Thermogenetic activation of Inka cells during heat stress accelerates copulation success. After a 3-hour heat-stress period during which Inka cells were thermogenetically activated in the final hour, time to successful copulation in ETH-Gal4>UAS-TRPA1 shortened relative to genetic controls. Blue, ETH-GAL4>UAS-TRPA1 (n=22); Orange, ETH-GAL4/ETH-GAL4 (n=20); Green, UAS-TRPA1/UAS-TRPA1 (n=19); Pink, Canton-S/Canton-S (n=18). Points show time to successful copulation events ± SE. Statistics: Pairwise comparisons used the log-rank (Mantel–Cox) test. Significance thresholds:; * $p<0.05$, *** $p < 0.001$.



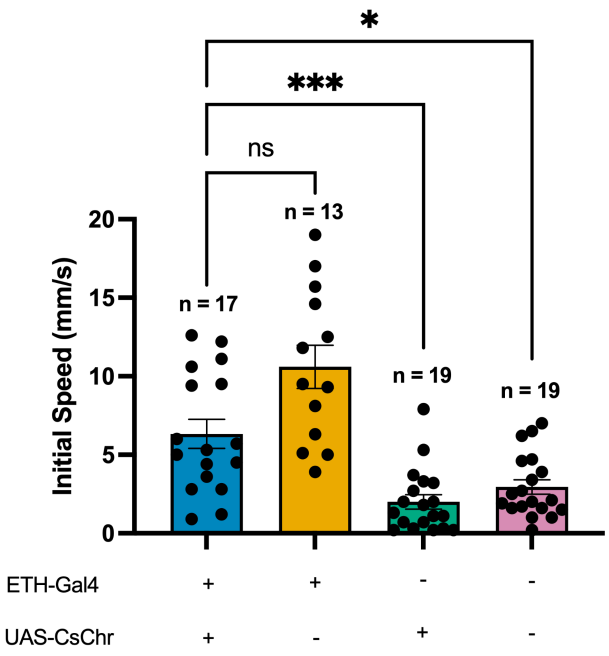
Group	Average Time to Courtship Initation ± SEM
ETH-Gal4>UAS-CsChr	12.12 ± 2.56s
ETH-Gal4	51.08 ± 15.49s
UAS-CsChr	157.88 ± 39.41s
Canton-S	50.60 ± 14.03s

Fig 8A. Optogenetic activation of Inka cells during heat stress decreases latency to courtship initiation. After a 3-hour heat-stress period during which Inka cells were optogenetically activated in the final hour, time to courtship initiation decreased in the ETH-Gal4>UAS-CsChrimson males relative to genetic controls. Table display average times to courtship initiation for each experimental group. Blue, ETH-Gal4>UAS-CsChrimson (n=17); Yellow, ETH-Gal4/ETH-Gal4 (n=12); Green, UAS-CsChrimson/UAS-CsChrimson (n=17); Pink, Canton-S/Canton-S (n=17). Bars show mean ± SEM. Statistics: Kruskal–Wallis test across groups followed by Dunn's multiple comparisons; * $p<0.05$, *** $p < 0.001$.



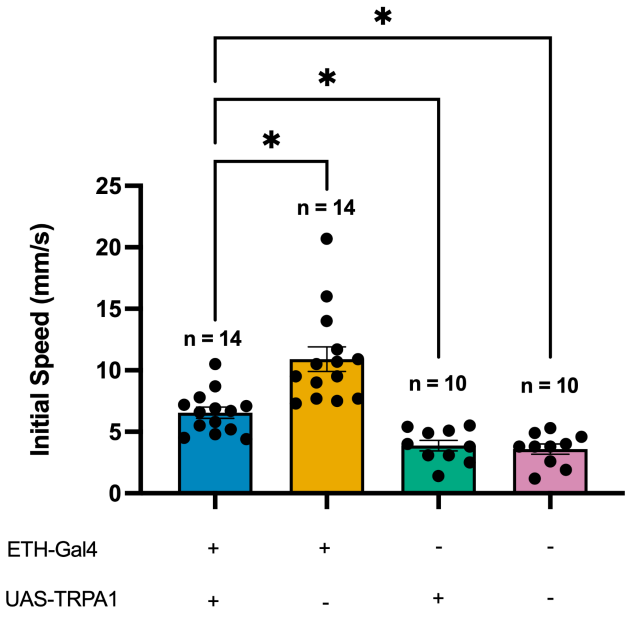
Group	Average Time to Courtship Initation ± SEM
ETH-Gal4>UAS-TRPA1	19.70 ± 3.92s
ETH-Gal4	72.94 ± 19.31s
UAS-TRPA1	38.95 ± 14.98s
Canton-S	82.60 ± 22.19s

Fig 8B. Thermogenetic activation of Inka cells during heat stress decreases latency to courtship initiation. After a 3-hour heat-stress period during which Inka cells were thermogenetically activated in the final hour, time to courtship initiation decreased in the ETH-Gal4>UAS-TRPA1 and UAS-TRPA1 males relative to genetic controls. Table display average times to courtship initiation for each experimental group. Blue, ETH-Gal4>UAS-TRPA1 (n=20); Orange, ETH-Gal4/ETH-Gal4 (n=18); Green, UAS-TRPA1/UAS-TRPA1 (n=20); Pink, Canton-S/Canton-S (n=15). Bars show mean ± SEM. Statistics: Kruskal–Wallis test across groups followed by Dunn's multiple comparisons; ns $p>0.05$, * $p<0.05$, ** $p<0.01$.



Group	Initial Speed ± SEM
ETH-Gal4>UAS-CsChr	6.3 ± 0.93 mm/s
ETH-Gal4	10.60 ± 1.37 mm/s
UAS-CsChr	2.00 ± 0.46 mm/s
Canton-S	2.95 ± 0.46 mm/s

Fig 9A. Optogenetic activation of Inka cells during heat stress normalizes motor phenotype. After a 3-hour heat-stress period during which Inka cells were optogenetically activated in the final hour, the initial speed of the UAS-CsChrimson and Canton-S males decreased, and the initial speed of the ETH-Gal4 males increased relative to the ETH-Gal4>UAS-CsChrimson males. Table display average initial speed for each experimental group. Blue, ETH-Gal4>UAS-CsChrimson (n=17); Yellow, ETH-Gal4/ETH-Gal4 (n=13); Green, UAS-CsChrimson/UAS-CsChrimson (n=19); Pink, Canton-S/Canton-S (n=19). Bars show mean ± SEM. Statistics: Kruskal–Wallis test across groups followed by Dunn's multiple comparisons; ns $p>0.05$, * $p<0.05$, *** $p < 0.001$.



Group	Initial Speed ± SEM
ETH-Gal4>UAS-TRPA1	6.41 ± 0.47 mm/s
ETH-Gal4	10.91 ± 1.01 mm/s
UAS-TRPA1	3.88 ± 0.43 mm/s
Canton-S	3.59 ± 0.42 mm/s

Fig 9B. Thermogenetic activation of Inka cells during heat stress normalizes motor phenotype. After a 3-hour heat-stress period during which Inka cells were thermogenetically activated in the final hour, the initial speed of the ETH-Gal4 males increased while the initial speed of both the UAS-TRPA1 and Canton-S males decreased relative to the ETH-Gal4>UAS-TRPA1 males. Table display average initial speed for each experimental group. Blue, ETH-Gal4>UAS-TRPA1 (n=14); Yellow, ETH-Gal4/ETH-Gal4 (n=14); Green, UAS-TRPA1/UAS-TRPA1 (n=10); Pink, Canton-S/Canton-S (n=10). Bars show mean ± SEM. Statistics: Kruskal–Wallis test across groups followed by Dunn's multiple comparisons; * $p<0.05$.

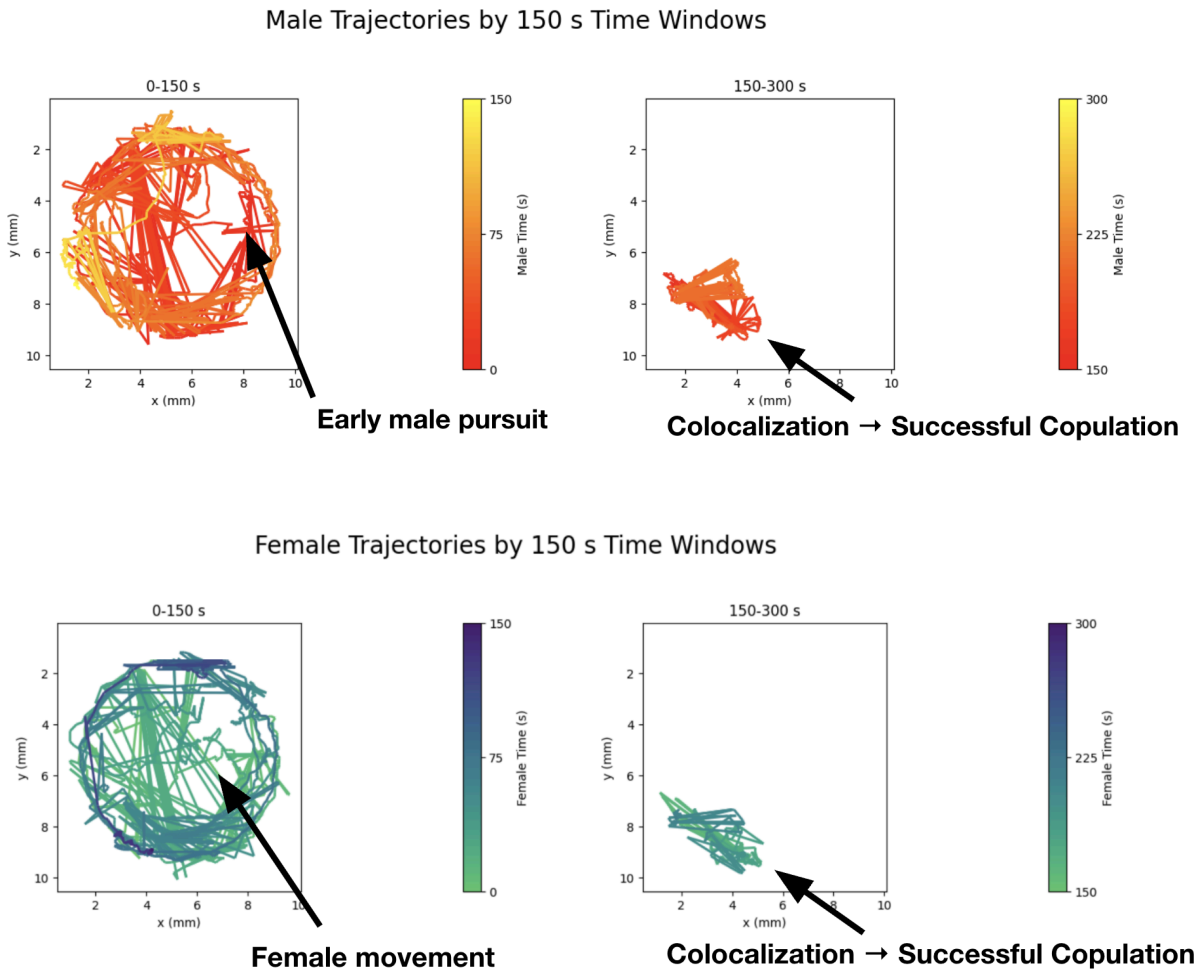


Figure 10A. Outcome 1: Successful copulation in ETH-Gal4>UAS-CsChrimson males. Representative male trajectory plot (top) and female trajectory plot (bottom) across two 150-second windows. Color scales represent elapsed time within each window (red to yellow for males, green to purple for females). During the first 150 seconds (left), the male engages in broad chamber exploration with directed pursuit while the female moves throughout the chamber. During the 150–300 second window (right), male and female trajectories converge into a tight region of the chamber, indicating spatial co-localization, and further sustained courtship engagement led to successful copulation.

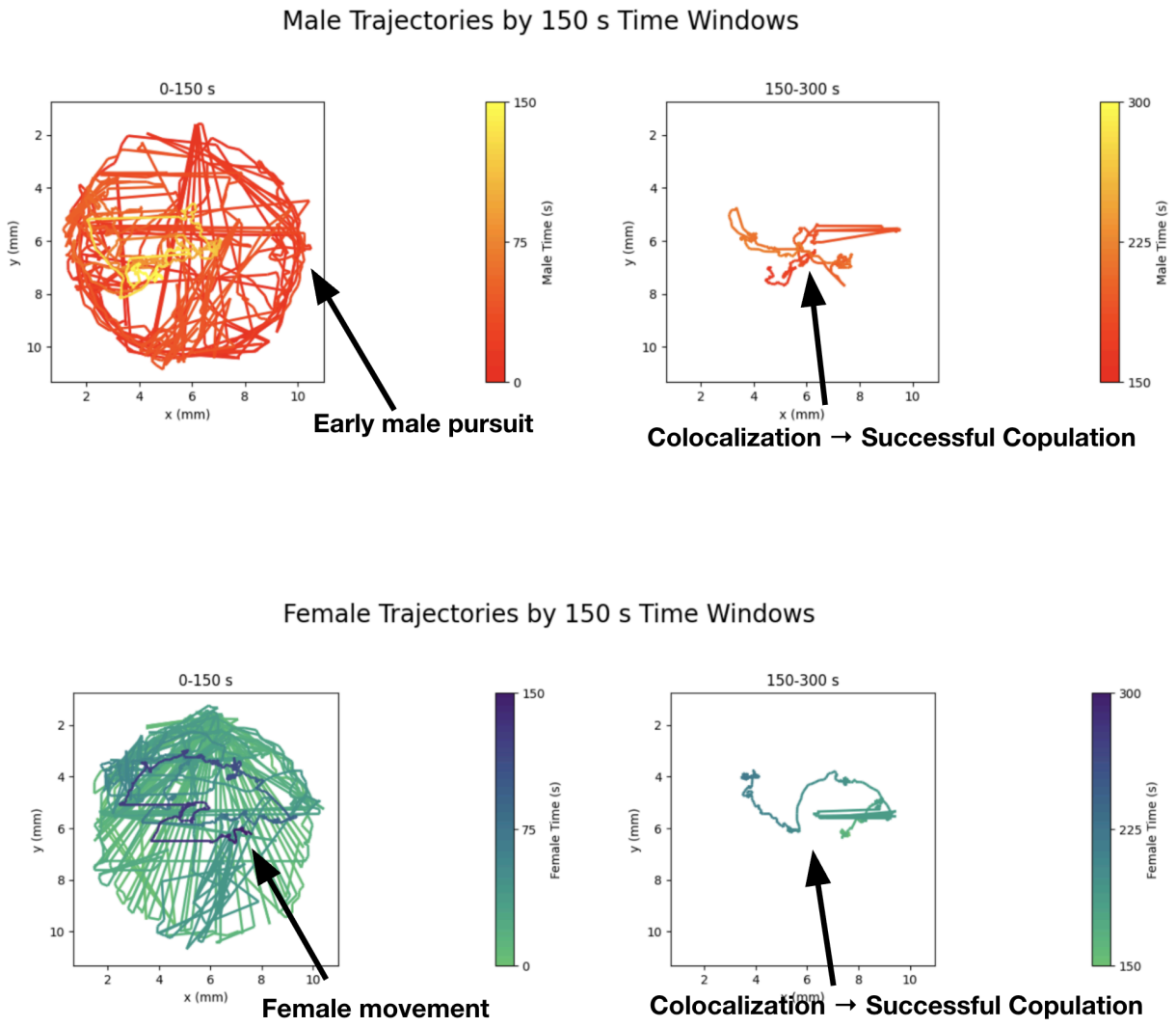


Figure 10B. Outcome 1: Successful copulation in ETH-Gal4>UAS-TRPA1 males. Representative male trajectory plot (top) and female trajectory plot (bottom) across two 150-second windows. Color scales represent elapsed time within each window (red to yellow for males, green to purple for females). During the first 150 seconds (left), the male engages in broad chamber exploration with directed pursuit while the female moves throughout the chamber. During the 150–300 second window (right), male and female trajectories converge into a tight region of the chamber, indicating spatial co-localization, and further sustained courtship engagement led to successful copulation.

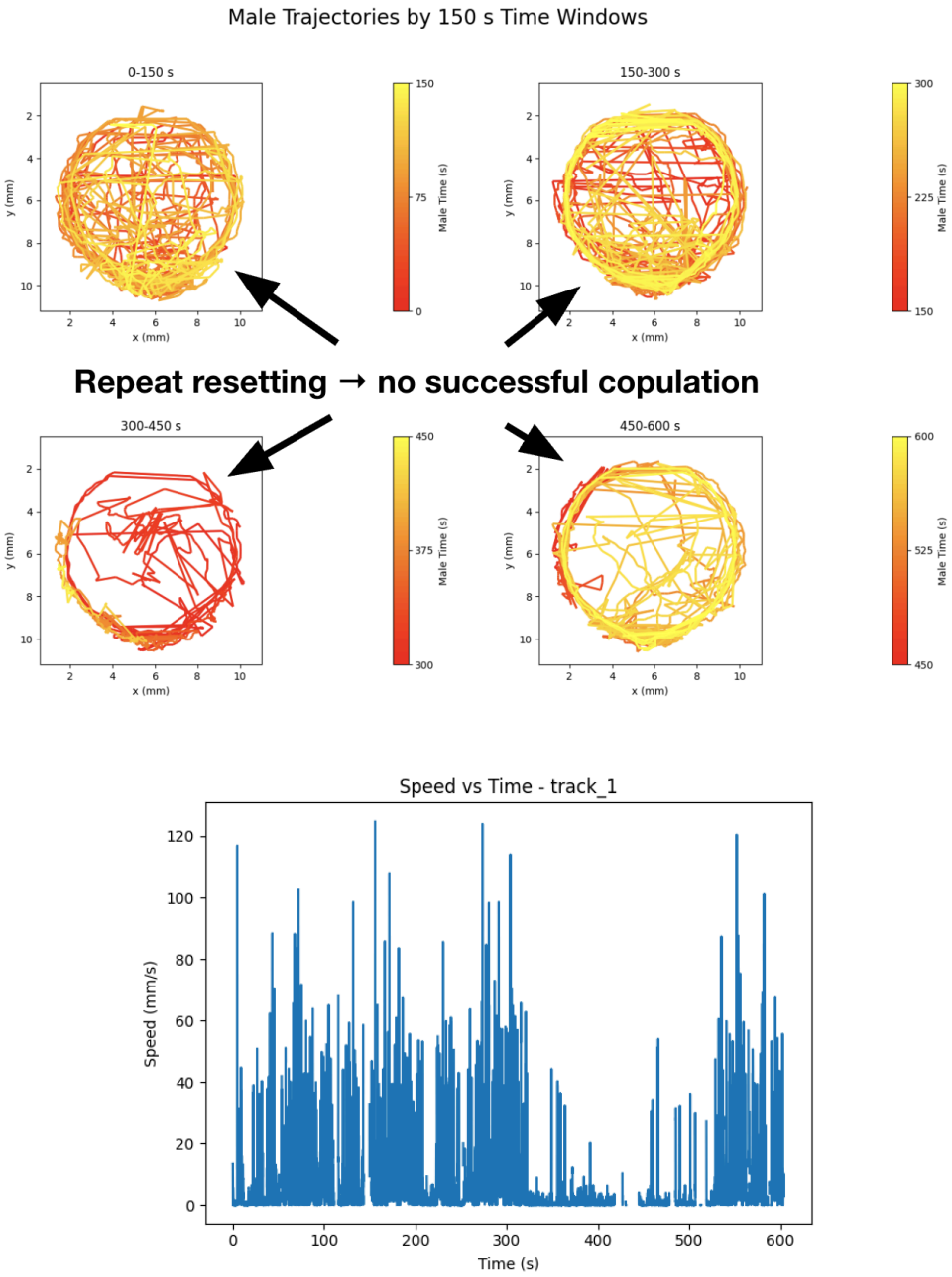


Figure 11A. Outcome 2: Repeated courtship resets in control males (optogenetic). Representative male trajectory plot (top) across four 150-second windows. Color scales represent elapsed time within each window (red to yellow). Multiple speed spikes (bottom) throughout the time period reflect repeated courtship attempts and resets.

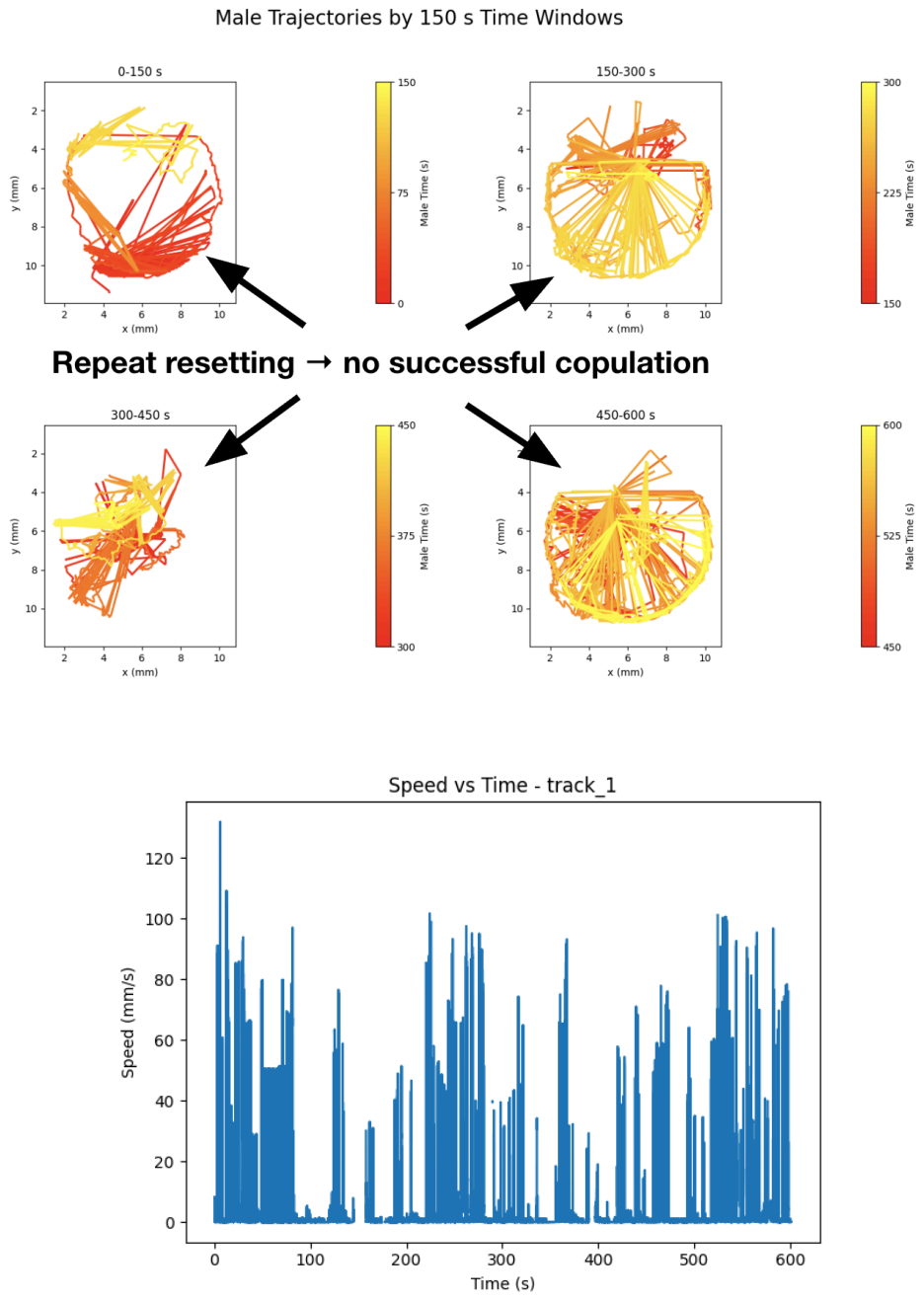


Figure 11B. Outcome 2: Repeated courtship resets in control males (thermogenetic). Representative male trajectory plot (top) across four 150-second windows. Color scales represent elapsed time within each window (red to yellow). Multiple speed spikes (bottom) throughout the time period reflect repeated courtship attempts and resets.

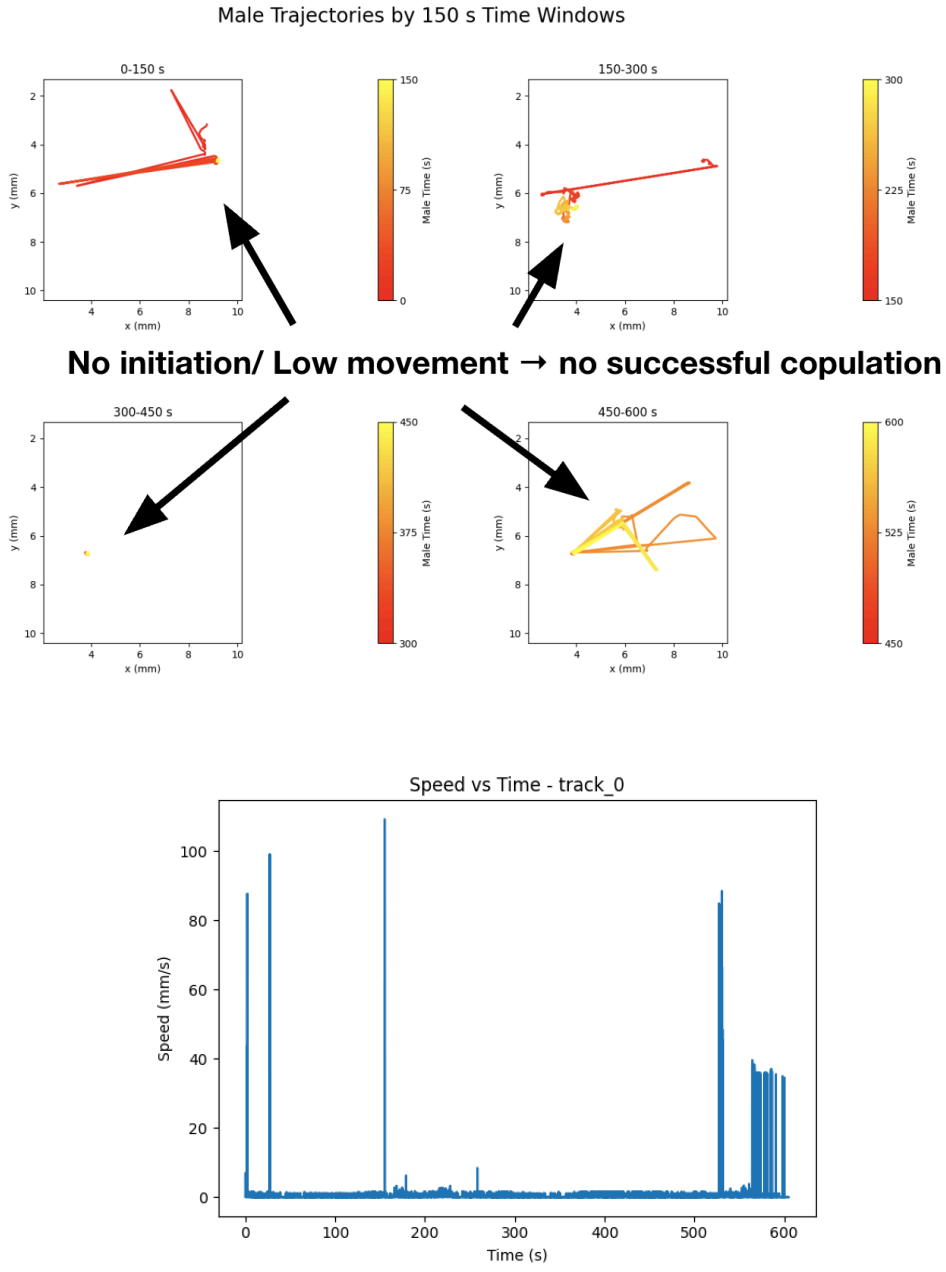


Figure 12A. Outcome 3: Failure of courtship initiation in control males (optogenetic). Representative male trajectory plot (top) across four 150-second windows. Color scales represent elapsed time within each window (red to yellow). Few speed spikes (bottom) throughout the time period reflect low courtship initiation.

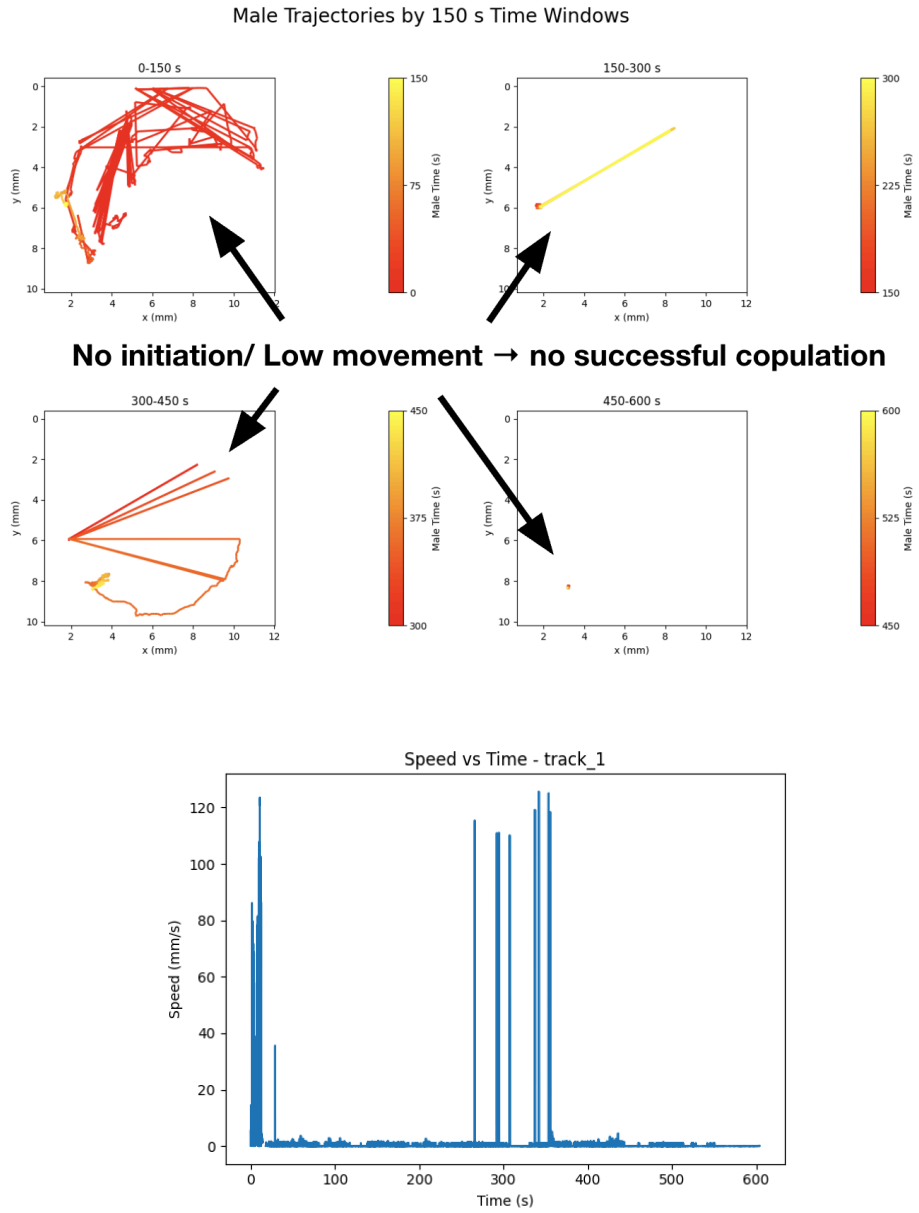


Figure 12B. Outcome 3: Failure of courtship initiation in control males (thermogenetic). Representative male trajectory plot (top) across four 150-second windows. Color scales represent elapsed time within each window (red to yellow). Few speed spikes (bottom) throughout the time period reflect low courtship initiation.

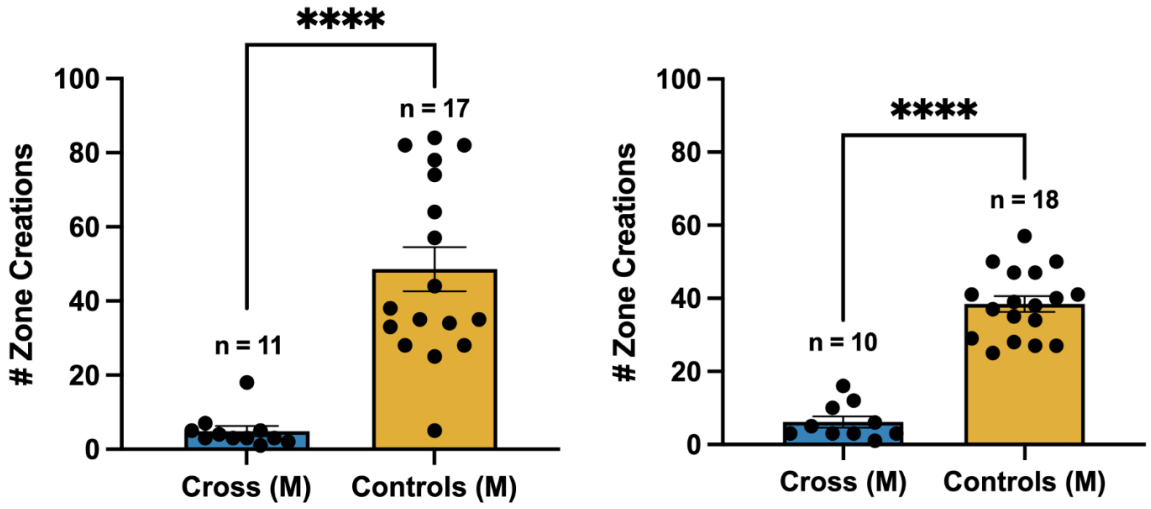


Fig 13. ETH-rescue males require fewer courtship attempts and resets. Number of zone creations during the 600-second observation window in ETH-rescue (Cross) and pooled control males in the optogenetic experiment (left) and the thermogenetic experiment (right). Cross males in both experiments produced significantly fewer zone creations than control males, indicating reduced courtship attempts and resets. The elevated zone creation count in control males reflects the repeated cycles of pursuit and disengagement characteristic of Outcome 2, which is driven by Unknown Factor X. Left: ETH-Gal4>UAS-CsChrimson Cross (n = 11) versus pooled controls (n = 17). Right: ETH-Gal4>UAS-dTRPA1 Cross (n = 10) versus pooled controls (n = 18). Bars show mean ± SEM. Statistics: Mann-Whitney U test; **** $p < 0.0001$.

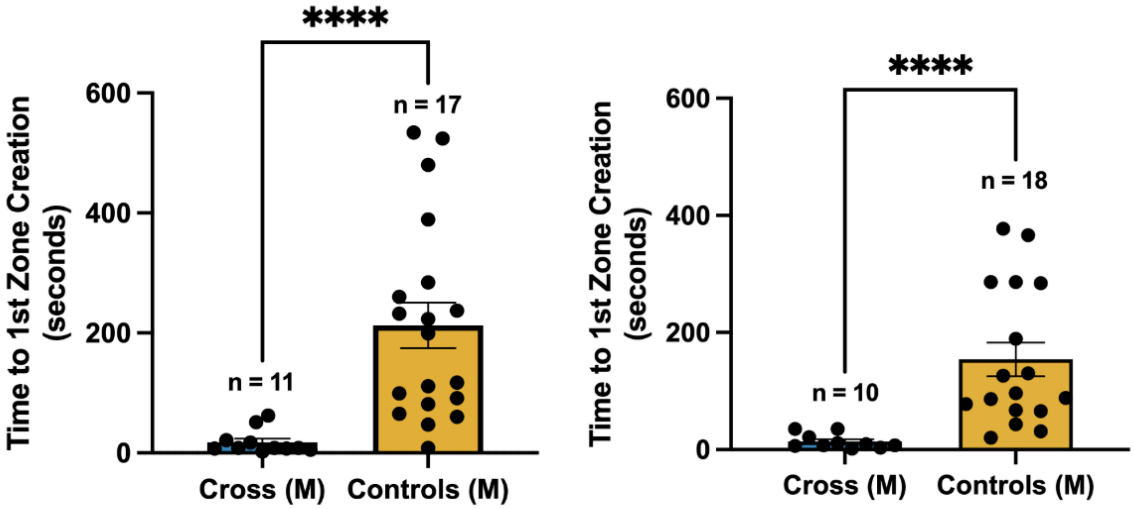


Fig 14. ETH-rescue males enter female proximity faster than controls. Time to first zone creation, defined as the latency from chamber loading to the male's first entry into a courtship-relevant zone around the female, in ETH-rescue (Cross) and pooled control males in the optogenetic experiment (left) and the thermogenetic experiment (right). Cross males in both experiments entered female proximity significantly faster than control males, indicating rapid courtship initiation. The pronounced delay in control males reflects the failure to localize to and approach the female characteristic of Outcome 3, driven by Unknown Factor Y. Left: ETH-Gal4>UAS-CsChrimson Cross (n = 11) versus pooled controls (n = 17). Right: ETH-Gal4>UAS-dTRPA1 Cross (n = 10) versus pooled controls (n = 18). Bars show mean ± SEM. Statistics: Mann-Whitney U test; **** $p < 0.0001$.

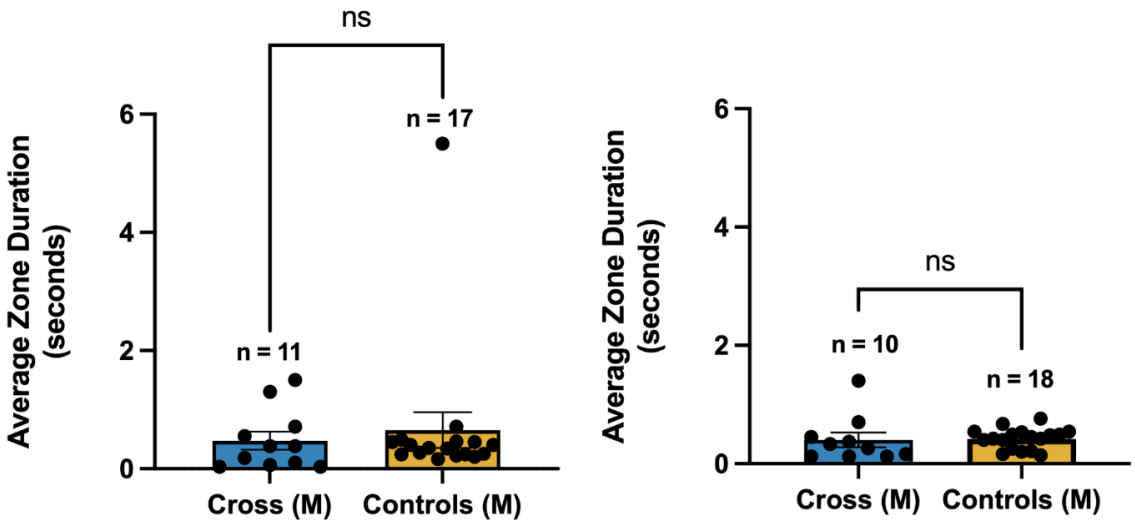


Fig 15. Female receptivity remained constant across treatment groups. Average zone duration, defined as the average time the female remained within courtship-relevant proximity per male zone entry, in ETH-rescue (Cross) and pooled control males in the optogenetic experiment (left) and the thermogenetic experiment (right). Average zone duration did not differ significantly between Cross and control pairs in either experiment, indicating that female receptivity remained comparable across treatment groups. The preservation of female receptivity in control pairs, despite their failure to achieve copulation, confirms that copulation failure is not attributable to female rejection but rather to male-side abnormalities driven by Unknown Factors X and Y. Left: ETH-Gal4>UAS-CsChrimson Cross (n = 11) versus pooled controls (n = 17). Right: ETH-Gal4>UAS-dTRPA1 Cross (n = 10) versus pooled controls (n = 18). Bars show mean ± SEM. Statistics: Mann-Whitney U test; ns $p > 0.05$.